RMetS

Royal Meteorological Society

Assessment of three dynamical urban climate downscaling methods: Brussels's future urban heat island under an A1B emission scenario

R. Hamdi,[a]* H. Van de Vyver,[a] R. De Troch[a,b] and P. Termonia[a,b]

[a] *Royal Meteorological Institute, Brussels, Belgium*
[b] *Department of Physics and Astronomy, Ghent University, Belgium*

ABSTRACT: A new high-resolution dynamical downscaling strategy to examine how rural and urban areas respond to change in future climate, is presented. The regional climate simulations have been performed with a new version of the limited-area model of the ARPEGE-IFS system running at 4 km resolution coupled with the Town Energy Balance (TEB) scheme. To downscale further the regional climate projections to a urban scale, at 1-km resolution, a stand-alone surface scheme is employed in offline mode. We performed downscaling simulations according to three model set-ups: (1) reference run, where TEB is not activated neither in 4 km simulations nor in 1 km urban simulation, (2) offline run, where TEB is activated only for 1 km urban simulation and (3) inline run, where TEB is activated both for regional and urban simulations. The applicability of this method is demonstrated for Brussels Capital Region, Belgium. For present climate conditions, another set of simulations were performed using European Center for Medium-Range Weather Forecasts global reanalysis ERA40 data. Results from our simulations indicate that the reference and offline runs have comparable values of daytime and nocturnal urban heat island (UHI) and lower values than the inline run. The inline values are closer to observations. In the future climate, under and A1B emission scenario, the three downscaling methods project a decrease of daytime UHI between −0.24 and −0.20 °C, however, their responses are different for nocturnal UHI: (1) reference run values remains unaltered, (2) for the offline runs, the frequency of present climate weak nocturnal UHI decreases to the benefit of negative UHIs leading to a significant decrease in the nocturnal UHI over the city and (3) for the inline run, nocturnal UHIs stays always positive but the frequency of the strong UHI decreases significantly in the future by 1 °C. The physical explanation is put forth. Copyright © 2013 Royal Meteorological Society

KEY WORDS   urban heat island; climate change; dynamical downscaling; TEB; Brussels

Received 25 September 2012; Revised 30 January 2013; Accepted 19 April 2013

1. Introduction

Today more than half of the human population lives in urban areas (Martine and Marshall, 2007) and by 2020 almost 80% of Europeans will live in urban areas. Since cities are emerging as first responders of climate change, scientists, urban planners and policy makers are beginning to work together in order to understand and monitor the interaction between urban areas and climate change and to consider adaptation and mitigation strategies (Rosenzweig *et al.*, 2010). To maintain or improve the quality of living in cities, urban planners need detailed information on future urban climate on the residential scale. However, because impervious surfaces cover only 0.34% of the world's land area (Sutton *et al.*, 2009), most of the global climate models (GCMs) that are utilized for climate change research do not account for urban surfaces (Best, 2006). The latest report

from the Intergovernmental Panel on Climate Change (IPCC, 2007) recognizes that urban warming in addition to greenhouse gas-induced warming has not explicitly been taken into account in climate change simulations. In fact, urban air temperatures are substantially higher than corresponding temperatures in the surrounding rural areas. This so-called urban heat island (UHI) effect that arises from changes in the radiative, thermal, moisture and aerodynamic properties is most pronounced for night-time minimum temperatures (Oke *et al.*, 1991). The influence of the UHI effect and its response to increased greenhouse-gas concentration has received little attention in the IPCC AR4 report (Christensen *et al.*, 2007).

In the last decade, increasingly sophisticated urban parameterizations were used to improve the representation of urban surface characteristics within the land surface models coupled to mesoscale atmospheric models. Numerous urban parameterization that simulate the surface energy and water balance of the urban canopy are described in the literature (see Masson, 2006 for a review) with varying levels of sophistication from relatively simplistic bulk approach (Lynn *et al.*, 2009) to single-layer

* Correspondence to: R. Hamdi, Royal Meteorological Institute, Avenue Circulaire, 3, B-1180 Brussels, Belgium.
E-mail: rafiq.hamdi@meteo.be

models (Masson, 2000; Kusaka *et al.*, 2001; Jin *et al.*, 2007) to the most sophisticated multi-layer schemes (Martilli *et al.*, 2002; Hamdi and Masson, 2008). Climate change modelling groups working at global scales are now beginning to implement urban parameterization within the land surface model component of their climate models. Recently, McCarthy *et al.*, (2010) included capability for sub-grid scale variation in surface properties, allowing multiple land surface types to occupy each GCM grid cell and an urban land surface scheme (Best *et al.*, 2006) has been included within the Hadley Centre Global Climate Model (HadAM3). In their study, McCarthy *et al.*, (2010) investigated the changes in the UHI intensity under doubled CO_2 conditions and anthropogenic heat scenarios using the HadAM3 atmosphere-only with prescribed sea surface temperature. Similarly, Oleson *et al.*, (2011) used the Community Atmosphere Model version 3.5 (CAM3.5) coupled to the Community Land Model-Urban (CLMU) to investigate UHI characteristics for present day through the end of the 21st century under an IPCC Fourth Assessment Report (AR4) A2 scenario. This study has been expanded in Oleson (2012) to analyse climate change simulations being performed for the IPCC AR5 as part of the Coupled Model Intercomparison Project 5 (CMIP5). Specifically, the response of urban and rural areas is computed for present-day conditions and three plausible trajectories of future climate conditions [Representative Concentration Pathway (RCPs)]: RCP8.5, PCR4.5, and RCP2.6; Moss *et al.*, (2010).

However, because of the coarse resolution of GCMs, climate change signals projected by GCMs may not capture certain mesoscale features of the UHI (Oleson *et al.*, 2011). In fact, UHIs can induce thermodynamically driven regional-scale flows (i.e. the UHI circulation). In calm or low wind conditions, the warmer air in the city core rises, pulling air near the surface radially inwards. A radially outward return flow may develop aloft. A dome of heated air often forms above the city. For slightly stronger ambient winds, a plume of heated air may extend downstream of the city transporting sensible heat between rural and urban areas (Hidalgo *et al.*, 2008). Similarly, heat islands in adjacent cities may interact on occasion through advection so as to increase the heat island intensity in the downwind city (Zhang *et al.*, 2009). Moreover, Guo *et al.*, (2006) and Zhang *et al.*, (2009) conducted case studies investigating the effects of urbanization in Beijing, China, on mesoscale convective precipitation events, and their results suggested that after urbanized modification, the surface latent heat flux is dramatically reduced because of the decrease in the moisture availability, while the sensible heat flux increases. This helps to decrease the convective available potential energy and the total precipitation in the whole domain, and especially in the urbanized region. Recently, Miao *et al.*, (2009) investigated the impacts of urban processes and urbanization on a localized, summer, heavy rainfall in Beijing using finescale simulations with the Weather Research and Forecasting model. The results confirm that urban surfaces tend to cause the rainfall to be more locally concentrated and that the city does play an important role in determining storm movements and rainfall amounts. All these features are not resolved in the aforementioned GCMs simulations. Another inherent limitation of these global climate simulations is that, traditionally, UHIs have been quantified by direct comparison of temperatures between two or more stations representing urban and rural references, but the global climate model cannot replicate such a diagnostic due to the coarse resolution in comparison to urban heterogeneity. Moreover, the atmospheric forcing (e.g. long-wave radiation) of these global climate simulations is prescribed identically over rural and urban surfaces that are within the same grid cell (McCarthy *et al.*, 2010; Oleson *et al.*, 2011). Furthermore, the urban class in these simulations is almost exclusively medium density which neglects the areas that may have the largest heat islands with high density and tall building district. These density classes are likely to be more relevant in distinguishing between the climate where people work and where people live (Oleson *et al.*, 2011).

Urban planners need climate scenarios including all the effects caused by local urban features. For this reason, techniques for downscaling global climate model simulations have been used. One of the most used techniques is based on the use of high-resolution regional climate models (RCM). Recently, McCarthy *et al.*, (2012) used the latest version of the Hadley Centre Regional Climate model HadRM3 at 25-km resolution coupled to a simple urban land-surface scheme (Best *et al.*, 2006) to assess the sensitivity of UK urban climates to large-scale greenhouse gas induced climate change, local forcing from urban land use, and anthropogenic heat flux resulting from energy use in urban areas. Kusaka *et al.* (2012a, 2012b) and Adachi *et al.* (2012) used the Weather Research and Forecast (WRF) model with a 3-km grid increment coupled to an urban canopy model to study the projected urban climate for the 2070s August, under SRES A1B scenario, in the three largest urban areas in Japan, Tokyo, Osaka and Nayoga. To further increase the horizontal resolution over urban areas, Früh *et al.* (2011) and Lemonsu *et al.* (2013) propose a method that firstly projects the global climate at the regional scale according to both dynamical and statistical downscaling techniques, and then simulates in offline mode the urban climate by using the specific urban climate model, MUKLIMO_3 and SURFEX-TEB, respectively. However, because of the offline mode of these simulations, the UHI signature is not included in the atmospheric forcing. Thus, the contribution and feedback processes by UHI and climate change are not taken into account when increasing the horizontal resolution. Therefore, in this study we propose a new dynamical downscaling method at 1-km horizontal resolution using the limited area version of the ARPEGE-IFS model, ALADIN (Bubnova *et al.*, 1995), coupled with the TEB single-layer urban canopy model (Masson, 2000). The applicability of the method is demonstrated for the Brussels Capital Region (BCR), centrally located in Belgium, with a size of $161.78 \, km^2$ and a registered

population of 1 031 215 on 1 January 2007, estimated by the National Institute of Statistics (INS, 2009).

2. Data and methods

2.1. Model descriptions

The atmospheric model used for the downscaling is ALARO (Gerard *et al*., 2009), which is a new version of the hydrostatic limited area ALADIN model with a revised and modular structure of the physical parameterization. In Gerard *et al*. (2009), a new approach was proposed, with an integrated sequential treatment of resolved condensation, deep convection and microphysics together with the use of prognostic variables. This new parameterization allows for the production of consistent and realistic results at resolutions ranging from few tens of kilometers down to less than 4 km (the so-called the grey zone, more details can be found in Gerard *et al*., 2009). It allows also handling feedback mechanisms present in nature and up to now only treated in models where the mesh size permits a fully explicit simulation of convective clouds. This new version is used operationally by the meteorological services of the Royal Meteorological Institute (RMI) of Belgium to make short-range high-resolution weather forecasts. Recently, this new version was tested in a regional climate reanalysis-driven simulation over Belgium (Hamdi *et al*., 2012a). The objective of this study was to explore the ability of high-resolution dynamical downscaling with the finest grid size of 4 km and sophisticated model physics scheme to better represent summer maximum surface air temperature over Belgium with emphasis on reproducing the extremes. This new version reduced considerably the original warm bias when using the diagnostic convective scheme based on Bougeault (1985), which suggests its ability to simulate weakly forced convective cloud in the summer over Belgium. It showed also that the consistent treatment of deep convection and cloud-radiation interaction when increasing the horizontal resolution is very important when studying high temperatures events. In this study, ALARO is used with the Foucart–Morcrette radiation scheme (Morcrette, 1991). It has a shortwave radiation scheme (Fouquart and Bonnel, 1980) with six spectral bands, whereas the longwave radiation is computed by the Rapid Radiative Transfer Model (RRTM) code (Mlawer *et al*., 1997).

The newly developed surface scheme of Météo-France SURFEX (SURface Externalisée; Le Moigne, 2009) has been implemented in ALARO relying on the algorithmic structure proposed by Best *et al*. (2004). SURFEX is an externalized surface scheme that can be run either in a coupled mode, in which case the atmospheric forcing is provided by the host atmospheric model (ALARO in our case), or in a stand-alone mode where the atmospheric drivers are derived either from observations or model output and fed to the surface scheme such that it is decoupled from the atmospheric part of a model. Therefore, no feedback exists between the surface and the upper air part of the atmosphere. In SURFEX, each grid box is made of four adjacent surfaces: nature, urban areas, sea or ocean and lake, associated with specific parameterization. Horizontal interaction does not exist between the different surface area tiles. The coverage of each of these surfaces in known through the global ECOCLIMAP database (Masson *et al*., 2003). Sea tiles use the Exchange Coefficients from Unified Multicampaigns Estimates (ECUME) parameterization (Belamari and Pirani, 2007). Inland waters use the classical formula of Charnock (1955). The interactions between soil, biosphere and atmospheric (ISBA) model (Noilhan and Planton, 1989) is used for vegetated areas and finally the TEB single-layer urban canopy model (Masson, 2000) is used for urban tiles. TEB is based on the canyon concept, where the town is represented with a roof, a road and two facing walls. The advantage is that relatively few individual surface energy balance evaluations need to be resolved, radiation interactions are simplified, and therefore computation time is kept low. Water, energy and momentum fluxes are computed by each parameterization and then aggregated at the grid-mesh scale according to the cover fraction of each tile. Recently, in the study of Hamdi *et al*., (2012b), the TEB scheme was implemented within ALARO running operationally at 4 km resolution. The primary question addressed was the ability of TEB to function at this relatively coarse resolution and, thus, assessing its potential use in an operational configuration to improve sensible weather performance over Belgium. The results show that promising improvements with a demonstrated positive impact are achieved by introducing TEB. The 2-m temperature and 2-m relative humidity improve compared to measurements in urban areas. Important urban characteristics, such as increased heat storage and Bowen ratio and the UHI effect, were successfully reproduced. In addition, comparison of wind speed and wind direction above the urban canopy indicate that the structure of the flow in urban areas is better reproduced with TEB.

2.2. Regional climate simulations

We utilize global climate scenarios from the ARPEGE-Climat (Gibelin and Déqué, 2003) GCM from Météo-France. Climate projections were produced within the FP6 ENSEMBLE project. We take the ARPEGE-Climat time slice 2071–2100 resulting from the IPCC SRES A1B scenario to estimate future change. Within this scenario, the mean temperature over Belgium is projected to increase by 3 °C at the end of the 21st century. For reference, the A1B scenario describes a future world of very rapid economic growth, global population that peaks in mid-century and declines thereafter, and the rapid introduction of new and more efficient technologies with a balance across fossil and non-fossil sources. The evaluation period 1961–1990 is chosen for the comparison of observations and simulation results. In addition, another set of simulations for the present climate conditions were performed using the European Center

for Medium-Range Weather Forecasts (ECMWF) global reanalysis ERA40 (Uppala *et al*., 2005), in which data assimilation methods are used to find optimal estimates for past atmospheric states that are consistent with meteorological observations and the model dynamics. This global reanalysis covers the last 40 years and can be used to provide the so-called perfect boundary conditions for RCMs and therefore to detect systematic biases of the RCM before simulating future climate change.

The first downscaling step in this study is accomplished using ALARO coupled with SURFEX in an inline mode. The spatial set-up is composed of two domains such as (1) a 40-km resolution parent domain with 80 × 80 grid points encompassing most of Western Europe (DOM1, Figure 1 top), (2) a 4-km one-way nested domain with its centre at 50.57°N, 4.55°E, with 181 physical grid points in the east–west and north–south directions (DOM2, Figure 1 top). An extra area of 11 points in both directions is added for the biperiodization of spectral fields for both domains where the configuration of the Davies formulation (Termonia *et al*., 2012). Both domains are vertically divided into 46 layers, separated by hybrid pressure terrain-following η levels (Simmons and Burridge, 1981). The height of the lower layer centre
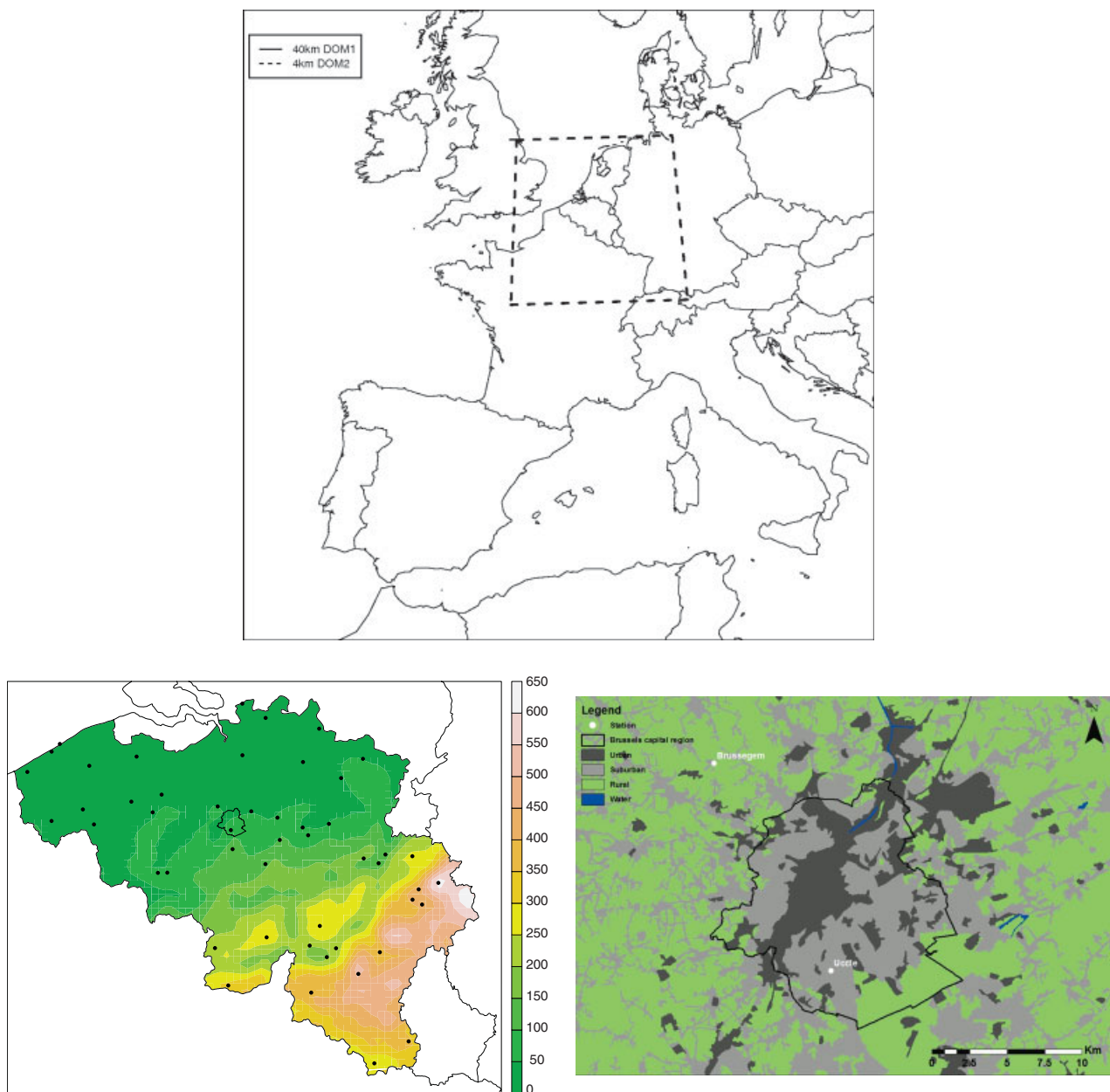

Figure 1. Top: Domains for the 4 km regional climate simulations, DOM1 represents the 40 km horizontal resolution, whereas DOM2 represents the nested domain with 4 km horizontal resolution. Bottom: Map of Belgium showing the topography (m) and the location of the 50 climatological stations and Study area of the Brussels Capital Region. The national recording station of the Royal Meteorological Institute of Belgium (Uccle, sub-urban station) and the rural station (Brussegem) are marked with a white circle.

is about 17 m above the ground. The time step is 300 and 180 s for the 40 and 4 km run, respectively. Our procedure is to interpolate the original coupling files (either ERA40 or ARPEGE-Climat) to 40-km resolution. These 6-h files serve as initial and boundary conditions for a 48-h run at 40-km resolution. These are started at 0000 UTC every day. The 3-hourly output from this first run serves as input for the high-resolution 4 km run. To avoid spin-up problems, the first 12 h are not taken into account. So we have 36 h of data left for the 4 km run which thus start at 12 UTC. Finally, we again dismiss the first 12 h of the runs, to arrive at 24 h of 1-hourly output at 4 km resolution. The benefit of frequent re-initialization is that it ensures the correct large-scale solution throughout the simulated period. It also prevents error growth in the form of a succession of convective scale interaction and feedbacks that, consistent with Lorenz's (1969) theoretical prediction can erroneously saturate the solution. In the study of Qian *et al*. (2003), it was shown that one should not let a regional model run unattended for a long period of time, after a number of days, the model diverges from the coupling data to arrive at some (constant) bias (Nicolis, 2003, 2004). However, the daily re-initialization will limit the equilibration of the surface physics (soil moisture and temperature), which is particularly desirable in long-term regional climate modelling (Giorgi and Mearns, 1999). Therefore, in this study, the soil variables evolve freely after initialization and are never corrected or nudged in the course of the simulation. This study focuses on the summer (June, July and August) months, when modelling of extremely high temperature events over Belgium strongly depends on the representation of interactions among atmospheric convection, clouds, radiation and land surface processes (Hamdi *et al*., 2012a). All simulations were initialized on 1 March and a 3-month spin-up period was used, before the start of the analysis on 1 June in each summer, in order to ensure model equilibrium between external forcing and internal dynamics, especially in terms of soil variables. The main greenhouse gases explicitly taken into account in the radiative model of ALARO are carbon dioxide (CO_2), methane (CH_4), nitrous oxide (NO_2) and chlorofluorocarbons CFC-11 and CFC-12. ALARO model uses the same gas concentrations as the ARPEGE-Climat. The concentration of greenhouse gases for the historical period is specified as annual mean values derived from observations and from IPCC A1B SRES scenario for the period 2071–2100.

2.3. Urban climate simulations

To downscale further the regional climate projections to an urban scale, enabling a simulation of a city and its surrounding, the SURFEX land surface modelling system is employed in offline mode. We selected a domain of 30×30 km covering the BCR and its immediate surrounding with 1 km spatial resolution (Figure 1 bottom). The present day land cover types contained in this domain includes 16 land-use land-cover classes provided by the ECOCLIMAP database. The urban areas are described according to eight different classes. The most important are the 'Dense urban' classes which cover the city centre of Brussels and the 'Temperate sub-urban' classes representing all residential areas located around the city centre of Brussels. The vegetation tiles around Brussels are composed of crops and temperate coniferous forest. For the vegetation tile, radiative, thermal and soil properties (*albedo*, roughness length, emissivity, thermal inertia, leaf area index, etc.) remain fixed through the simulation. For the urban tile, geometrical, thermal and radiative properties of roofs, walls and roads were set to value representing the contemporaneous setting and are kept constant for all simulations (Table I). Another important urban-related aspect is the anthropogenic heat. This term includes all heat emitted by human activities: traffic, release from industry and release from residential buildings. Over the area presented in this study, release from buildings has been shown to be the dominant component of the anthropogenic heat (Van Weverberg *et al*., 2008). Therefore, all anthropogenic heats from industry and traffic were set to zero. TEB has an internal building temperature model that permits climate-controlled internal temperatures to interact with the natural climate outdoors. To mimic space heating/cooling a fixed minimum internal buildings temperature of 19 °C is specified (Pigeon *et al*., 2008).

Since SURFEX is run in offline mode a set of atmospheric forcing must be provided. This forcing data consists of 1-hourly: air temperature, specific humidity, atmospheric pressure, incoming global radiation, incoming longwave radiation, precipitation rate, and wind speed and direction, derived from the 4 km resolution regional climate simulations described in the previous section. These data are then temporally interpolated to get data with the time resolution of the integration scheme of SURFEX (300 s). The forcing produced in the previous section are with a spatial resolution of 4 km only, while the ultimate goal is to perform urban climate simulations at 1 km spatial resolution. The 4 km resolution atmospheric forcing are simply projected on the 1 km grid by searching for the closest grid point.

For the offline run, SURFEX is coupled to a surface boundary layer (SBL) scheme following the methodology described in Hamdi and Masson (2008), Masson and Seity (2009), and Hamdi *et al*. (2009). With this version, six prognostic air layers (0.5, 2, 4, 6.5, 10 and 17 m above the ground) are added from the ground up to the forcing level (which is the lowest ALARO level at 17 m). The SBL is, thus, resolved prognostically, taking into account large-scale forcing, turbulence, and if any, drag and canopy forces. The interest of this approach is to use the advanced physical description of the SBL-canopy interactions that was available only in complex coupled multilayer surface scheme in offline surface schemes (Masson and Seity, 2009) for more details). All SURFEX-SBL prognostic variables are initialized using the initial value of the drivers derived from the regional climate simulations.

Table I. Three-dimensional morphometric parameters of the 'Dense urban' and the 'Temperate sub-urban' classes used to represent the city of Brussels and the physical properties of urban elements used in the model (from ECOCLIMAP, Masson *et al*., 2003).

	Dense urban			Temperate sub-urban		
Morphometric parameters						
Building height (m)		30			10	
Building fraction		0.5			0.5	
Canyon aspect ratio		1			0.5	
Wall-plane area ratio		1			0.5	
Roughness length (m)		3			1	
Road properties						
Sky view factor		0.41			0.62	
Albedo		0.08			0.08	
Emissivity		0.94			0.94	
Depth of layers, 1 (nearest to surface), 2, and 3 (m)	0.05	0.1	1	0.05	0.1	1
Heat Capacity (MJ m^{-3} K^{-1})	1.94	1.28	1.28	1.94	1.28	1.28
Thermal conductivity (W m^{-1} K^{-1})	0.75	0.25	0.25	0.75	0.25	0.25
Roof properties						
Albedo		0.15			0.15	
Emissivity		0.90			0.9	
Depth of layers, 1 (nearest to surface), 2, and 3 (m)	0.05	0.4	0.1	0.05	0.4	0.1
Heat Capacity (MJ m^{-3} K^{-1})	2.11	0.28	0.29	2.11	0.28	0.29
Thermal conductivity (W m^{-1} K^{-1})	1.51	0.08	0.05	1.51	0.08	0.05
Wall properties						
Sky view factor		0.29			0.38	
Albedo		0.25			0.25	
Emissivity		0.85			0.85	
Depth of layers, 1 (nearest to surface), 2, and 3 (m)	0.02	0.12	0.05	0.02	0.12	0.05
Heat Capacity (MJ m^{-3} K^{-1})	1.55	1.55	0.29	1.55	1.55	0.29
Thermal conductivity (W m^{-1} K^{-1})	0.93	0.93	0.05	0.93	0.93	0.05

2.4. Experimental design

The experiment includes nine 30-years simulations, which are detailed in Table II. The downscaling strategy presented in the previous sections is first applied to the past climate conditions 1961–1990 in order to evaluate the methodology. The meteorological conditions at lateral boundaries were taken either from ERA40 (ERA_) or from ARPEGE-Climat present conditions (ARP_). The ALARO model was driven with ERA40 reanalysis data to test model performance and to evaluate consistency with the ARPEGE-Climat driven results. The future climate 2071–2100 simulations (A1B_) are computed using the IPCC SRES A1B scenario of ARPEGE-Climat.

To examine the contribution and feedback processes between UHI and regional climate for present and future conditions, we performed regional and urban climate simulations with and without TEB. For the simulations without TEB, urban areas are considered simply as rock and the ISBA scheme is used for all grid points of the domain. We performed downscaling simulations according to three model set-ups:

- The reference '_RF' run representing a control simulation where the TEB scheme is not activated neither in the 4 km regional climate simulation nor in the 1 km urban climate simulation.

Table II. Description of the numerical experiments.

		Regional climate simulation		Urban climate simulation	
		Rock	TEB	Rock	TEB
ERA40	1961–1990				
	ERA_RF	yes			
	ERA_OF	yes		yes	yes
	ERA_IN		yes		yes
ARP	1961–1990				
	ARP_RF	yes		yes	
	ARP_OF	yes			yes
	ARP_IN		yes		yes
A1B	2071–2100				
	A1B_RF	yes		yes	
	A1B_OF	yes			yes
	A1B_IN		yes		yes

- The offline '_OF' run where the TEB scheme is activated only for the 1 km urban climate simulation. This run mimics the situation where the atmospheric forcing coming from the regional climate simulations did not include any signature of the UHI.
- The inline 'IN' run where the TEB scheme is activated both for the regional and urban climate simulations.

2.5. Station data

Regional climate simulations for the present climate are validated against an observational database retrieved from the climatological network of the RMI. It consists of daily minimum (T_MIN) and maximum (T_MAX) temperature time series from 50 stations geographically dispersed around Belgium (Figure 1 bottom) and representing the conditions for a mixture of both coastal and inland locations. The climatological network is nowadays composed by more than 250 stations. However, in order to have a homogeneous network without a substantial interruption during the period 1961–1990, only 50 stations were selected. Measurements provided by this climatological network have been extensively used for recent climatological analysis (Hamdi and Van de Vyver, 2011; Van de Vyver, 2012; Hamdi *et al*., 2012a).

The strength of the UHI of BCR is estimated using the daily minimum and maximum temperature time series observed at Uccle, the national recording station of the RMI and at a rural meteorological station, Brussegem, situated 20 km far away from the centre of Brussels (see Figure 1 bottom). Uccle is situated some 6 km south of the centre of the capital in a suburban area (50.80°N, 04.35°E). The Brussegem station is located outside the area influenced by the UHI of Brussels (Van Weverberg *et al*., 2008, their Figure 5) and is not influenced by the Southwest-prevailing wind direction. The annual surface air temperature in Uccle has increased by 1.4 °C during the 20th century (Yan *et al*., 2002), which substantially exceeds the global average of 0.74 °C/100 years (IPCC, 2007). The effects of the Brussels's UHI on observed surface temperature at Uccle have been investigated from observations and numerical simulations. Hamdi *et al*. (2009) and Hamdi and Van de Vyver 2011 indicated that 45% of the overall warming trend is attributed to intensifying Brussels's UHI effects, due to urbanization around the station, rather than to changes in local/regional climate.

3. Results and discussion

3.1. Evaluation of the regional climate simulation

Fifty time series are extracted from each model simulation using the nearest grid point selection method. Each temperature time series is then corrected to fit the same altitude as the nearest observation series. This has been done by adding the standard atmosphere gradient of 6.5K/km to the original model temperature values,
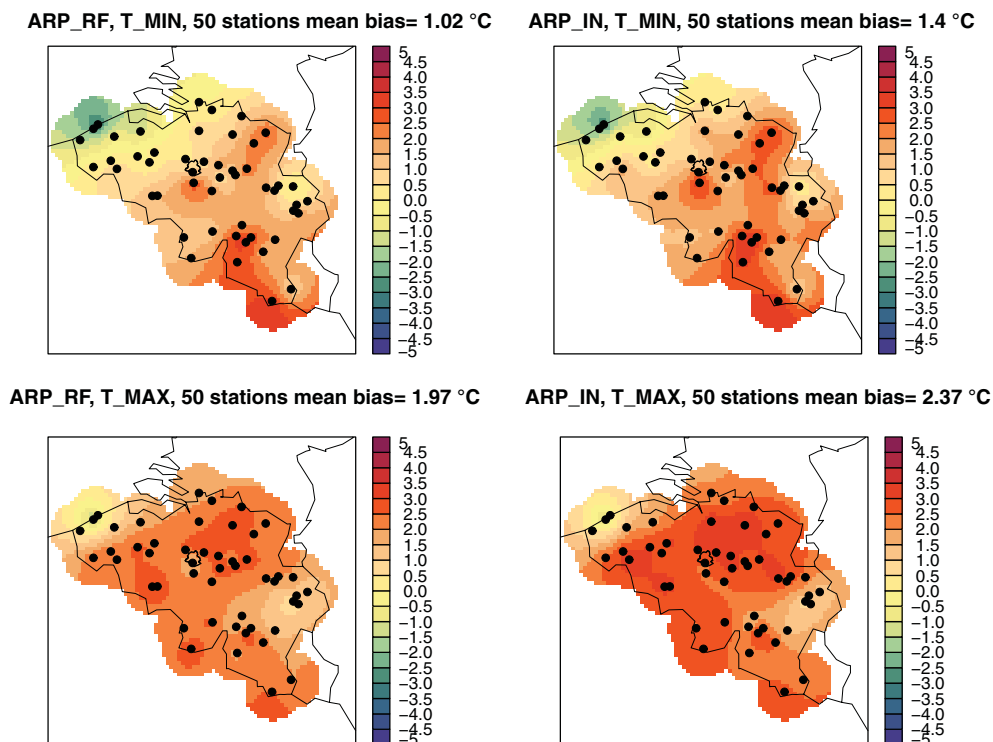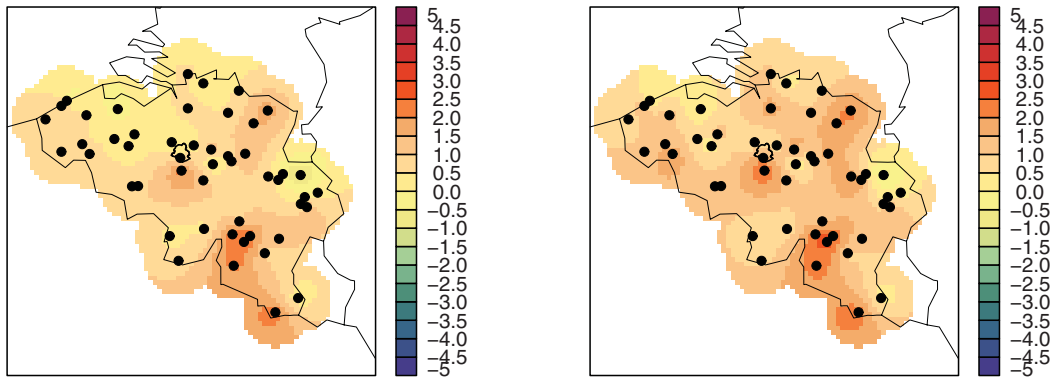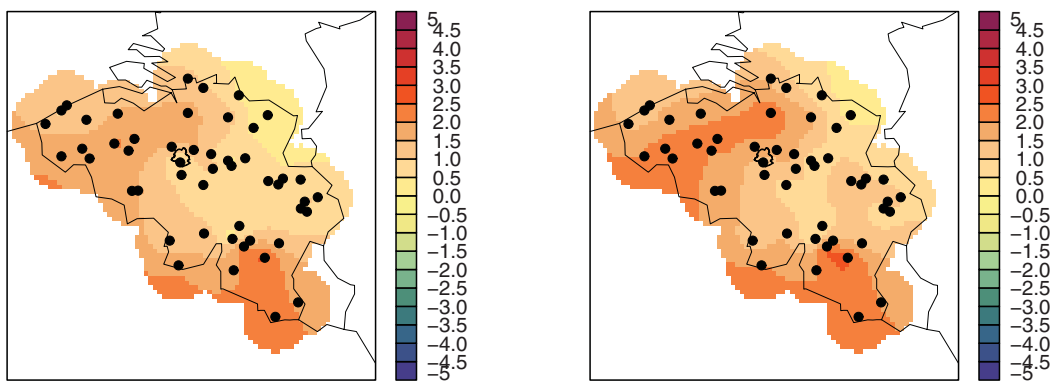

Figure 2. Spatial distribution of 30-year average summer bias (°C) (model minus observed) of the daily minimum (top) and maximum (bottom) temperature obtained with ARP_RF (left column) and ARP_IN (right column). The mean bias over the 50 climatological stations is indicated at the top of each sub-figures.

ERA_RF, T_MIN, 50 stations mean bias= 0.77 °C   **ERA_IN, T_MIN, 50 stations mean bias= 1.15 °C**

ERA_RF, T_MAX, 50 stations mean bias= 1.2 °C   **ERA_IN, T_MAX, 50 stations mean bias= 1.48 °C**

Figure 3. Spatial distribution of 30-year average summer bias (°C) (model minus observed) of the daily minimum (top) and maximum (bottom) temperature obtained with ERA_RF (left column) and ERA_IN (right column). The mean bias over the 50 climatological stations is indicated at the top of each sub-figures.

according to the altitude difference between the model grid point and the observational station. Figures 2 and 3 show the 30-year average summer bias of daily minimum and maximum temperature that were obtained by comparing the ERA40 (ERA_RF and ERA_IN) and ARPEGE (ARP_RF and ARP_IN) driven simulations, respectively, to observations from the 50 climatological stations. Figure 4 shows the 30-year average summer root mean square error of daily minimum and maximum temperature and Table III presents the correlation coefficient that were obtained by comparing the ERA40 driven simulations to observations from the 50 climatological stations.
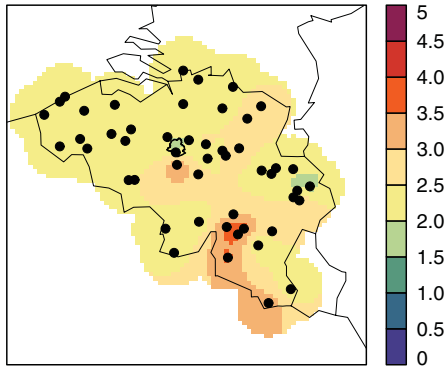
3.1.1. *Minimum temperature*

In term of mean values, the ERA_RF simulation captures well the minimum temperature with positive bias less than 1 °C over Belgium and less than 0.5 °C over the BCR. The ARP_RF values are higher than observed particularly in central Belgium where the bias over the BCR is now about 1 °C. The ARPEGE-Climat driven experiment also exhibits another significant cold bias (−1.5 °C) near the coast which is not corresponding to the warm bias in the ERA40 experiment. The introduction of TEB in the regional climate simulations increases the

warm bias for both ERA40 and ARPEGE-Climat driven experiments. The average bias increases by 0.40 °C over the BCR for both ERA_IN and ARP_IN simulations.
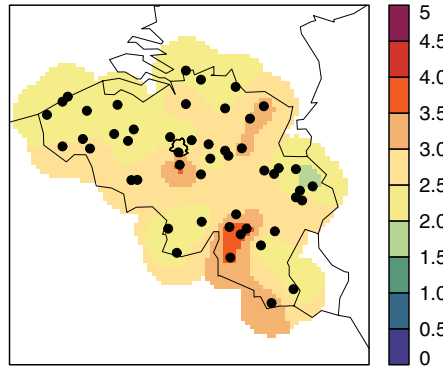
3.1.2. *Maximum temperature*

The ARP_RF values are higher than observed particularly in Flanders and central Belgium where warm bias exceeds 2 °C. ERA_RF produces values much closer to observed over the whole country, reducing the overall average biases to 1.2 °C. The difference of the average bias over the 50 climatological stations between the ARP_RF and ERA_RF simulation and observations is 0.25 °C for minimum temperature and 0.77 °C for maximum temperature. Therefore the error magnitude in summer T_MAX tends to be larger than T_MIN, indicating that the correct simulation of T_MAX is more challenging in summer for the ARPEGE-Climat driven experiments. Previous downscaling studies for other geographical areas have shown error magnitudes comparable to or larger than those computed in this study (Lim *et al.*, 2007; Caldwell *et al.*, 2009; Lynn *et al.*, 2010; Paquin-Ricard *et al.*, 2010). The introduction of TEB in the regional climate simulations increases the warm bias for both
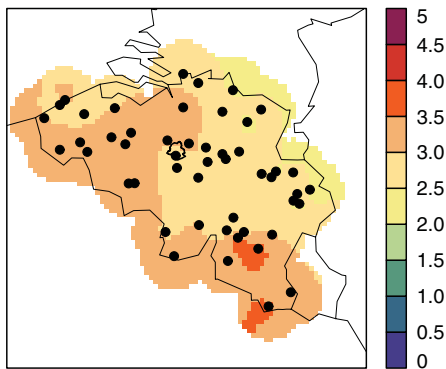
ERA_RF, T_MIN, 50 stations mean RMSE= 2.44 °C

ERA_IN, T_MIN, 50 stations mean RMSE= 2.61 °C

ERA_RF, T_MAX, 50 stations mean RMSE= 2.93 °C

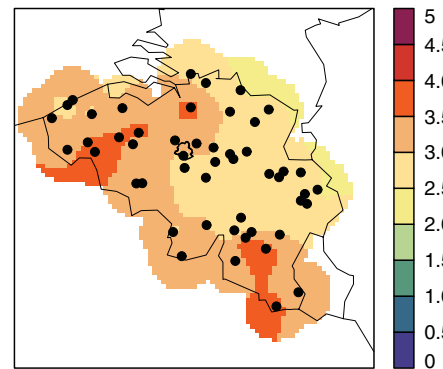**ERA_IN, T_MAX, 50 stations mean RMSE= 3.02 °C**

Figure 4. Spatial distribution of 30-year average summer root mean square error (RMSE) (°C) of the daily minimum (top) and maximum (bottom) temperature obtained with ERA_RF (left column) and ERA_IN (right column). The mean RMSE over the 50 climatological stations is indicated at the top of each sub-figures.

Table III. The 30-year average correlation coefficient of daily minimum and maximum temperature that were obtained by comparing the ERA40 driven simulations to observations and averaging over the 50 climatological stations.

	T_MIN	T_MAX
ERA_RF	0.72	0.82
ERA_IN	0.71	0.82

ERA40 and ARPEGE-Climat driven experiments by 0.40 °C over the BCR.

3.2. Present climate UHI characteristics

The UHI is defined as the difference between the urban canopy air temperature and the minimum air temperature in the surrounding rural areas. This difference is analysed for daily minimum and maximum temperature also referred to as the nocturnal and daytime UHIs, respectively.

3.2.1. Spatial aspect

3.2.1.1. Nocturnal UHI: Nocturnal UHI is of particular interest because of its potential impacts on human health.

In fact, warmer urban night-time temperatures may exacerbate the severity of heat waves because they limit relief from heat stress during daytime (Changnon *et al*., 1996). Figure 5 presents the spatial distribution of the 30-year average BCR's nocturnal UHI for the ARPEGE-Climat and ERA40 driven experiments. It is apparent that both the reference and offline runs have lower values for the BCR's nocturnal UHI values than the ones calculated by the inline run. In fact, while the use of TEB in offline mode increases the UHI value at the city centre of BCR by only 0.26 and 0.4 °C with respect to the reference run for ARP_OF and ERA_OF, it is increased by 0.85 and 1.08 °C for ARP_IN and ERA_IN, respectively. It can further be noticed that the ARP_IN and ERA_IN runs has a comparable magnitude of the BCR's nocturnal UHI (2.5 °C at the city centre) and a similar pattern even if the ARPEGE-Climat driven experiment has a warmer bias than the ERA40 driven simulations. Figure 5 shows that the highest values occur in the centre of the city, while the values gradually decrease towards the outskirts of the BCR. This can be explained by: (1) the higher heat capacity of the large buildings, which, in combination with the lower *albedo*, delays the cooling compared with the environment (more explanation can be found in
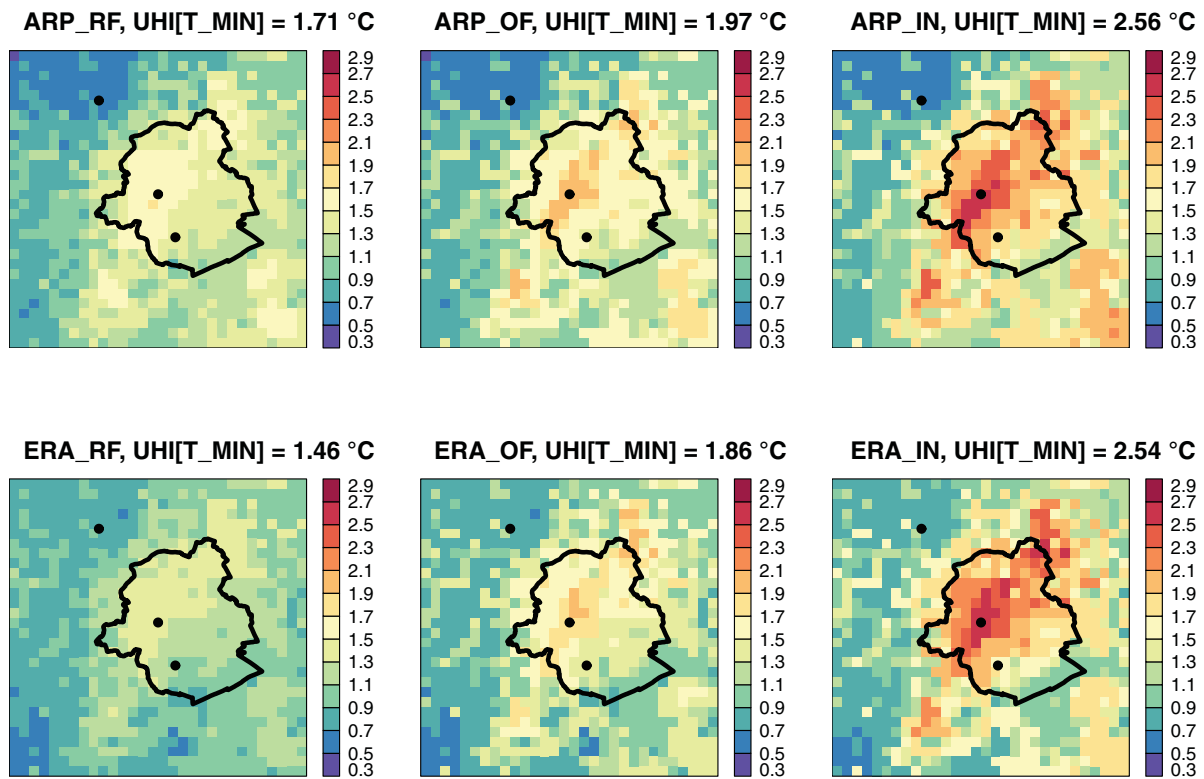
Figure 5. Spatial distribution of 30-year, 1961–1990, average BCR's nocturnal UHI (°C) for the ARPEGE-Climat (top) and ERA40 (bottom) driven experiments. The three columns correspond to the reference, offline and inline runs. The black circles indicates the location of centre of Brussels, the Uccle station situated some 6 km south of the centre of the capital in a suburban area, and the rural Brussegem station situated 20 km far away from the centre of Brussels. The UHI in the centre of the domain is indicated at the top of each sub-figure.

Hamdi and Schayes (2008)), (2) radiation trapping effects in street canyon and (3) the limited evapotranspiration which prevents evaporative cooling of urban areas.

3.2.1.2. Daytime UHI: Figure 6 presents the spatial distribution of the 30-year average BCR's daytime UHI for the ARPEGE-Climat and ERA40 driven experiments. It is apparent that the UHI is predominantly a nocturnal phenomenon in the model in agreement with observations (Hamdi *et al.*, 2009; Hamdi and Van de Vyver, 2011). For example, for the inline runs the nocturnal UHI is more than two times the daytime UHI. Just as found for the nocturnal UHI, both the reference and offline runs have comparable values, about 0.8–0.9 °C at the city centre, but give lower values for the BCR's daytime UHI than the ones calculated by the inline run. Also, all ERA40 and ARPEGE-Climat driven experiments have comparable magnitude of the BCR's daytime UHI (1.2 °C at the city centre for the inline run) and a similar pattern even if the error magnitude of the ARPEGE-Climat driven simulations in summer T_MAX tends to be larger that T_MIN. Contrarily to what is found for the nocturnal UHI, the daytime UHI in the suburban areas is higher than in the city centre for the inline runs in agreement with previous studies (Trusilova *et al.*, 2008; Früh *et al.*, 2011; Lemonsu *et al.* 2013). This is caused by the partial shading of street canyons (due to small sky view factor) leading to urban cooling. Urban surfaces (roads, walls)

that are not exposed to direct sunlight during the hottest daytime hours keep street canyons cooler than open suburban areas. It can further be noticed that the daytime UHI is lowest in the south-eastern part of the BCR. This can be explained by to the presence of the Sonian Forest (see Figure 1 bottom) which lies in the south of Brussels. Forest, urban parks, and garden improve the thermal environment of the urban areas through shading, evapotranspiration and cool-air production (Pearlmutter *et al.*, 2009; Hassan and Mahmoud, 2011; Peters *et al.*, 2011; Goldbach and Kuttler, 2013). One can notice that this cooling effect, simulated by the inline runs, is also observed in the neighbouring developed suburban areas of the Sonian Forest, in agreement with previous studies (Eliasson, 1996; Ng *et al.*, 2012). This feature is not reproduced neither with the reference nor with the offline run while the inline run reproduce it very well.

3.2.2. The UHI at Uccle

3.2.2.1. Time series: The nocturnal and daily UHI intensity is defined as the difference in minimum and maximum, respectively, temperature between Uccle and the rural station Brussegem. The summer mean of each year between 1955 and 2006 is plotted with the linear trends in Figure 7 (unfortunately no data were found for Brussegem between 1972 and 1979). The UHI calculated in the period 1961–1990 with the ARPEGE-Climat
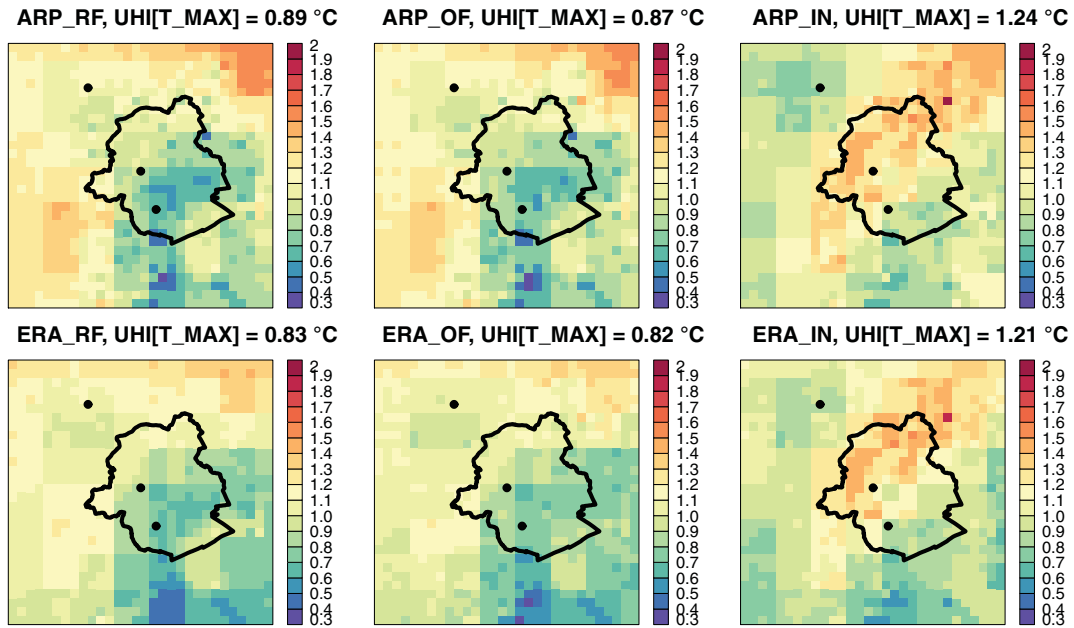
ARP_RF, UHI[T_MAX] = 0.89 °C **ARP_OF, UHI[T_MAX] = 0.87 °C** **ARP_IN, UHI[T_MAX] = 1.24 °C**

ERA_RF, UHI[T_MAX] = 0.83 °C **ERA_OF, UHI[T_MAX] = 0.82 °C** **ERA_IN, UHI[T_MAX] = 1.21 °C**

Figure 6. Spatial distribution of 30-year, 1961–1990, average BCR's daytime UHI (°C) for the ARPEGE-Climat (top) and ERA40 (bottom) driven experiments. The three columns correspond to the reference, offline and inline runs. The black circles indicates the location of centre of Brussels, the Uccle station situated some 6 km south of the centre of the capital in a suburban area, and the rural Brussegem station situated 20 km far away from the centre of Brussels. The UHI in the centre of the domain is indicated at the top of each sub-figure.
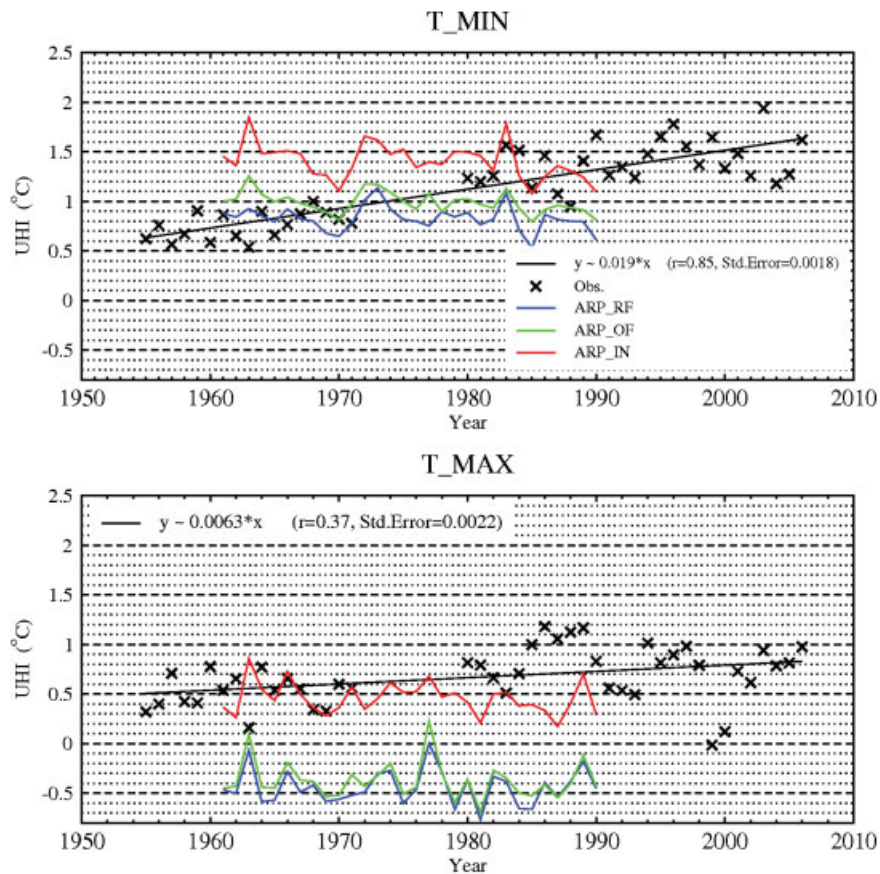
Figure 7. Time series (1955–2006) of the summer-mean UHI (°C) at Uccle for the minimum (top) and maximum (bottom) temperature estimated as the difference between Uccle and the rural station Brussegem with the linear trend (*r* is the correlation coefficient and Std.Error is the standard error of the regression coefficient, no data were found for Brussegem between 1972 and 1979). Also shown are the UHI calculated in the period 1961–1990 with the ARPEGE-Climat driven simulations for the reference (ARP_RF), offline (ARP_OF), and inline (ARP_IN) runs.

Table IV. Mean nocturnal (UHI_N) and daytime (UHI_D) urban heat island for 1961–1970 and 1981–1990 from observations and ERA40 and ARPEGE-Climat driven experiments.

		1961–1970		1981–1990		Δ	
		UHI_N	UHI_D	UHI_N	UHI_D	UHI_N	UHI_D
Obs		0.80	0.51	1.32	0.90	0.52	0.39
Reference	ARP_RF	0.82	−0.45	0.78	−0.47	−0.04	−0.02
	ERA_RF	0.45	−0.43	0.44	−0.24	−0.01	0.19
Offline	ARP_OF	1.00	−0.37	0.93	−0.42	−0.07	−0.05
	ERA_OF	0.73	−0.34	0.70	−0.17	−0.03	0.17
Inline	ARP_IN	1.43	0.47	1.31	0.40	−0.12	−0.07
	ERA_IN	1.23	0.25	1.20	0.43	−0.03	0.18

Δ refers to the difference between the two periods.

driven simulations for the reference (ARP_RF), offline (ARP_OF), and inline (ARP_IN) runs are also plotted.

As indicated by Figure 7, the observed UHI on minimum temperature is shown to be rising at a higher rate (2.85) than on maximum temperature with a linear trend of 0.19 °C ($\pm$ 0.02 °C) and 0.06 ($\pm$ 0.02 °C) (10 year)$^{-1}$. This is due to the increased urbanization around the Uccle station (Hamdi and Van de Vyver, 2011). Daytime UHI seems to be substantially less affected by urbanization which is consistent with previous studies (Kalnay and Cai, 2003; Hua *et al*., 2008; McCarthy *et al*., 2010, Fischer *et al*., 2012). The visual verification of Figure 7 shows that the ARP_OF and ARP_IN runs have a tendency to produce higher nocturnal UHI for the period 1961–1970. The average mean for the ARPEGE-Climat driven runs is significantly warmer with an average of 0.82 °C for ARP_RF, 1 °C for ARP_OF and 1.43 °C for ARP_IN *versus* 0.80 °C observed (Table IV). However, for the period 1981–1990, the ARP_IN nocturnal UHI agree very well with the observations, with an average value of 1.31 *versus* 1.32 °C observed, while the two other runs (ARP_RF and ARP_OF) result in much lower values with 0.78 and 0.93 °C, respectively. The lack of changes in urban extent and properties in the model simulations explains this discrepancy since the UHI is calculated under static, present-day urban conditions. The increase in the observed nocturnal UHI over the two periods (about 0.52 °C) is not reproduced neither by the ARPEGE-Climat nor by the ERA40 driven experiments (Table IV). The nocturnal UHI declines in ARP_IN but remains about the same in ERA-IN.

In contrast to the nocturnal UHI, the ARP_RF and ARP_OF runs are comparable and produce negative values for the daytime UHI while the ARP_IN values are much higher and close to the observations with an average value of 0.47 *versus* 0.51 °C observed for 1961–1970 and 0.40 *versus* 0.90 °C observed for the 1981–1990 decade. However, the increase in the observed daytime UHI over the two periods (about 0.39 °C) is not reproduced by ARP_IN. The daytime UHI declines in ARP_IN but increases significantly in ERA_IN (Table IV). Oleson (2012) examined how urban and rural areas might respond differently to changes in climate using a new parameterization of urban areas in the Community Climate System Model version 4 (CCSM4). They found that

the daytime UHI is steadily until about 1960 when it begins to decline as the slope of the CO_2 time series increases.

It can be further noticed that the urban simulations using TEB in offline mode results in an underestimation of nocturnal and daytime UHI. This result is in agreement with recent studies by Früh *et al*. (2011) and Lemonsu *et al*. (2013) who proposed a method that firstly projects the global climate at the regional scale according to both dynamical and statistical downscaling techniques, and then simulates in offline mode the urban climate.

3.2.2.2. Extreme heat islands: Extreme UHIs are of concern because they exacerbate summer heatwave, leading to increased mortality amongst sensitive members of the population as evidence by the summer of 2003 (Sardon, 2007). The nocturnal and daytime UHI at Uccle simulated by the ARPEGE-Climat and ERA40 driven experiments are compared to the observations according to the quantile-quantile method. The comparison is done over the period 1981–1990 for the nocturnal UHI and over the whole period for the daytime UHI. The results are presented in Figures 8 and 9, respectively. As evident, the reference run underestimates the warm extremes of both the nocturnal and daytime UHI by about 2 °C. The underestimation of the nocturnal UHI is greatly reduced to less than 0.5 °C with the offline runs. However, for the daytime UHI, the offline runs reproduce the same extreme value statistics of the reference runs for both the ARPEGE-Climat and ERA40 driven experiments. The inline values are much closer to the observations especially the ARP_IN run where the daytime UHI warm extremes are well simulated. For the nocturnal UHI extremes, the inline runs compare correctly against observations until the 97.5% quantile where a slight overestimation of about 0.5 °C is noted for the warm extremes. An overestimation of the negative nocturnal UHI values is, however, simulated with the inline runs. However, exact compatibility is not to be expected because with the 4 km horizontal resolution of the climate drivers used to run SURFEX, we are not able to replicate the micrometeorology in the required details. Figures 7–9 provide evidence that the climatological behaviour of the UHI in the inline run in response to large-scale dynamic is broadly consistent with observations.
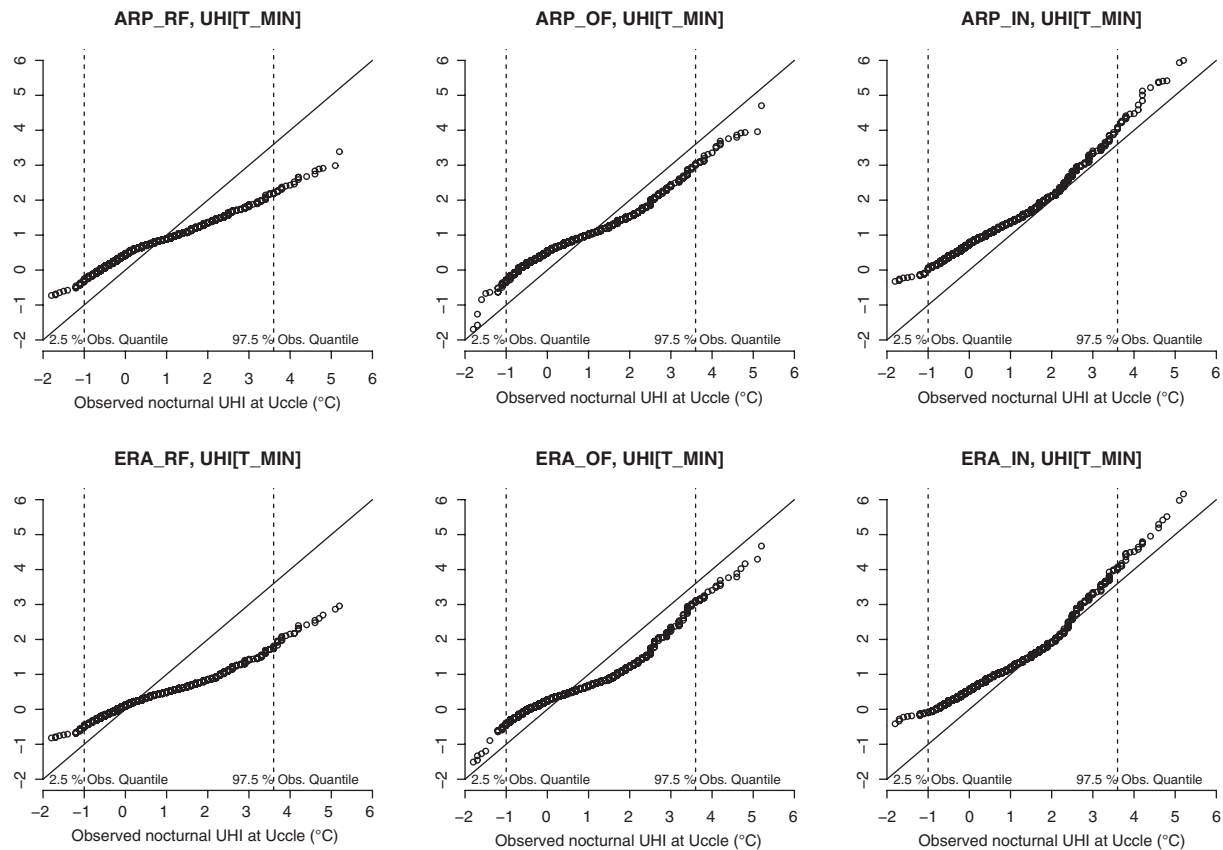
Figure 8. Quantile–quantile comparison between the nocturnal UHI (°C) at Uccle from observations and from the ARPEGE-Climat (top) and ERA40 (bottom) driven experiments for the period 1981–1990. The three columns correspond to the reference, offline, and inline runs. The vertical dashed lines present the 2.5 and 97.5% quantile of the observations.

3.3. Future UHI characteristics

Table V presents the 30-year average T_MIN and T_MAX over the present climate and under an A1B emission scenario for the city centre of Brussels, the suburban (Uccle) and rural (Brussegem) station. In Table VI, we present an estimation of the 20-year return level difference between present and future climate for T_MIN and T_MAX using Peak-Over-Thresholds (POT) method (Coles, 2001; Hamdi *et al*., 2012a). Because of long-term climate changes, we have implemented a non-stationary POT-model as in Kyselý *et al*. (2010). A time dependent threshold was estimated using the quantile regression methodology (Koenker and Bassett, 1978; Koenker, 2005). Figure 10 presents the 2071–2100 minus 1961–1990 spatial distribution of the 20-year return level difference (°C) of T_MIN and T_MAX. Both the city and rural areas warm substantially in response to greenhouse induced climate change. It is more important for T_MAX than T_MIN (about +2.7 °C *vs* +2.0 °C for the inline run, respectively, see Table V). The comparison between the three land-cover classes indicates, however, that the city centre warms less than the suburban and rural areas for T_MIN and T_MAX and for the offline and inline runs. The lowest increase in temperature is noted for T_MIN with the offline run, it reaches +1.85 °C for the city centre of Brussels against +2.18 °C at the rural station Brussegem. This will reduce the urban to rural contrast.

Just as found in Lemonsu *et al*., (2013), the high rural temperatures are linked with a soil dryness during the summer where the projected cumulated summer precipitation over the BCR decreased in the regional climate simulations by 35% both with A1B_RF and A1B_IN runs (a detailed study about the projected precipitation with and without TEB will be published in a subsequent paper).

Figure 11 presents the 2071–2100 minus 1961–1990 spatial distribution of 30-year average nocturnal and daytime UHI and Figure 12 presents a quantile–quantile comparison between the nocturnal and daytime UHI at the city centre of Brussels from ARP_ and A1B_ ARPEGE-Climat driven experiment.

3.3.1. Nocturnal UHI

Compared to the magnitude of the warming in response to greenhouse induced climate change, changes in the nocturnal UHI magnitude are small. The nocturnal UHI simulated by the reference run remains unaltered (see Figure 11 top-left). Also, there is no change in either the frequency or magnitude of the extreme heat islands (see Figure 12 top-left). McCarthy *et al*. (2012) obtained similar results for the city of London using a simple urban land-surface scheme where the urban tile is a modification of the vegetation canopy model, and the modified urban parameters are surface *albedo*, roughness
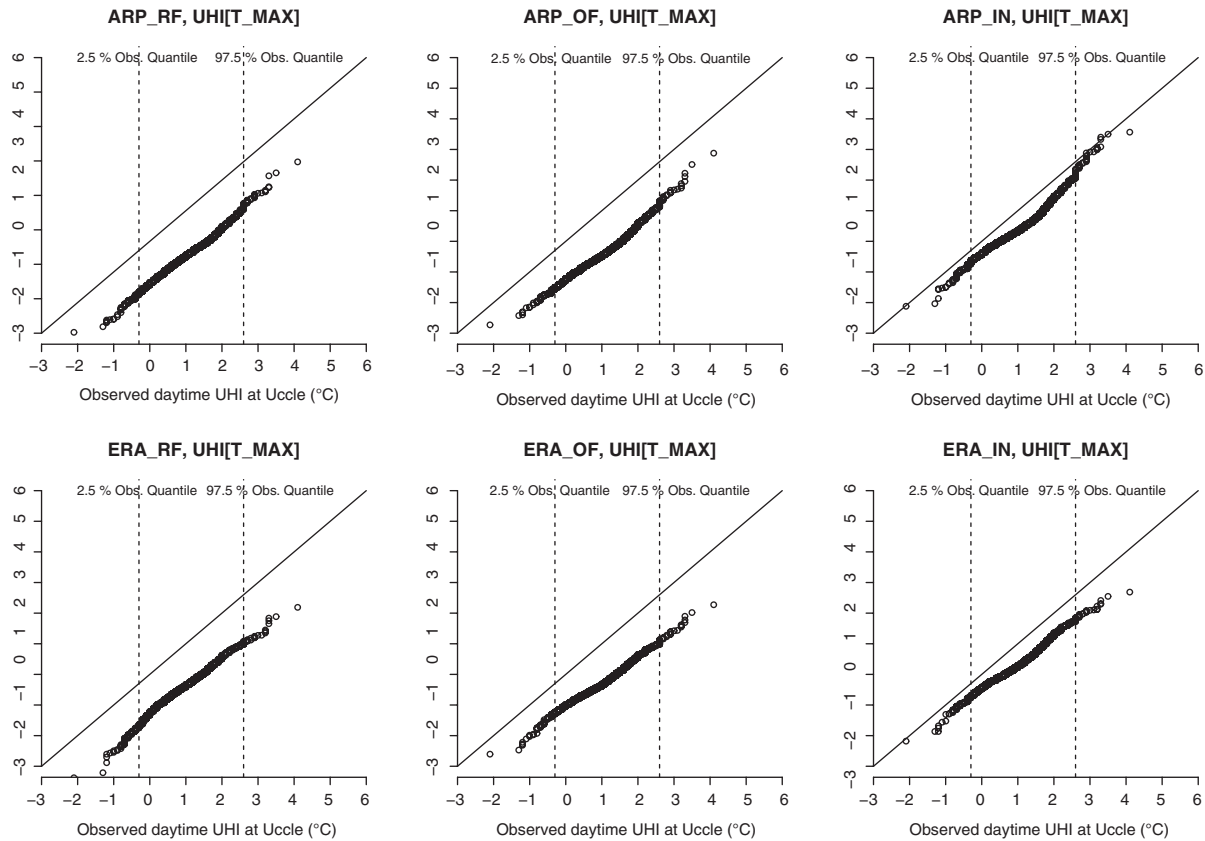
Figure 9. Quantile–quantile comparison between the daytime UHI (°C) at Uccle from observations and from the ARPEGE-Climat (top) and ERA40 (bottom) driven experiments for the period 1961–1990. The three columns correspond to the reference, offline and inline runs. The vertical dashed lines present the 2.5 and 97.5% quantile of the observations.

Table V. Thirty-year average T_MIN and T_MAX over present and under an A1B scenario for the city centre, suburban and rural stations and for the reference, offline, and inline runs with the ARPEGE-Climat driven experiments.

		T_MIN			T_MAX		
		1961–1990	2071–2100	Δ	1961–1990	2071–2100	Δ
Reference	City centre	14.08	16.26	2.18	23.62	26.41	2.79
	Suburban (Uccle)	13.76	15.98	2.22	23.32	26.21	2.89
	Rural (Brussegem)	13.01	15.19	2.18	23.83	26.60	2.77
Offline	City centre	14.36	16.21	1.85	23.62	26.30	2.68
	Suburban (Uccle)	13.94	15.90	1.96	23.40	26.19	2.79
	Rural (Brussegem)	13.01	15.19	2.18	23.83	26.60	2.77
Inline	City centre	15.21	17.21	2.00	24.63	27.27	2.64
	Suburban (Uccle)	14.65	16.71	2.06	24.59	27.32	2.73
	Rural (Brussegem)	13.32	15.48	2.16	24.18	26.89	2.71

Δ refers to the difference between the two periods.

length of momentum, the ratio of roughness lengths of heat and momentum, and heat capacity. Contrarily to what is found for the reference run, the offline run (see Figure 11 top-centre) presents a significant decrease in the nocturnal UHI over the city centre (−0.36 °C) and the suburban areas (−0.28 °C) while there is an increase over the rural areas and the Sonian Forest in the southeast of Brussels. Thus, rural areas are warming more than urban at night. Lemonsu *et al*. (2013) found somewhat higher value with a nocturnal UHI 1 °C weaker at the end of the 21st century over the city of Paris using the same offline modelling strategy. Figure 12 (top-centre) shows

that the frequency of present climate weak nocturnal UHI (between 0 and 1 °C) decreases to the benefit of negative UHIs in the future climate. Just as it is found in Oleson *et al*. (2011), the mechanism by which this occurs is related to changes in incoming long-wave radiation at night. Figure 13 presents the summer-mean diurnal average of 2071–2100 minus 1961–1990 surface energy fluxes from the offline runs at the city centre of Brussels, the Uccle suburban station, and the Brussegem rural station. At night, there is an increase in incoming long-wave radiation in the future time slice compared to present climate. The nocturnal net radiation increases

Table VI. Estimation of 20-year return level difference (°C) between present (1990) and future climate (2100) of T_MIN and T_MAX for the city centre, suburban and rural stations and for the reference, offline, and inline runs with the ARPEGE-Climat driven experiments.

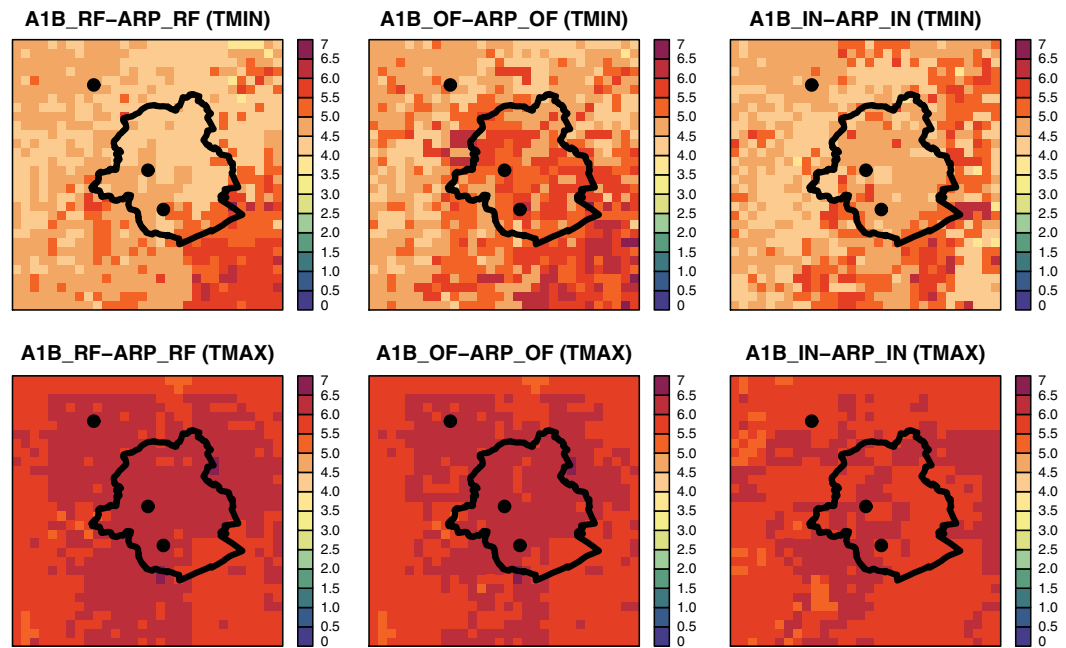|	T_MIN			T_MAX		
	Reference	Offline	Inline	Reference	Offline	Inline
City centre	4.44	5.32	4.50	6.15	6.12	6.00
Suburban (Uccle)	4.58	5.95	4.76	6.08	6.01	6.05
Rural (Brussegem)	4.41	4.41	4.50	6.23	6.23	5.60

Figure 10. 2071–2100 minus 1961–1990 spatial distribution of the 20-year return level difference (°C) of T_MIN (top) and T_MAX (bottom). The three columns correspond to the reference, offline and inline runs. The black circles indicates the location of centre of Brussels, the Uccle station situated some 6 km south of the centre of the capital in a suburban area, and the rural Brussegem station situated 20 km far away from the centre of Brussels.

at 0100 UTC by 15 and 10 W m^{-2} for the city centre and the suburban Uccle station, respectively. However, the larger storage capacity of urban areas buffers the increase in long-wave radiation. Sensible heat flux is reduced accordingly so that urban air temperature warms less than rural air temperature. In contrast, rural areas have a smaller storage term and warm more in response to the increased long-wave radiation. The analysis confirms results of Oleson *et al*. (2011) that rural areas warm more than urban areas at night when incoming long-wave radiation is increased. We notice that Oleson *et al*. (2011) used a single-layer urban parameterization similar to the TEB scheme used in the present study.

In the inline run (see Figure 12 top-right), the nocturnal UHIs are always positive with values between 0 and 7 °C in the present climate. The same range is detected in the future climate. However, the frequency of the strong UHI (>3 °C) decreases significantly in the future climate by 1 °C. These results are directly connected to the high temperatures simulated in rural areas correlated with soil drying, confirming the results of Lemonsu *et al*. (2013).

In fact, the differential effects of increased atmospheric long-wave radiation on urban and rural areas was not simulated with the inline run as it can be clearly seen from the summer-mean diurnal average of 2071–2100 minus 1961–1990 surface energy fluxes presented in Figure 14. These results indicate that the offline run exacerbates the decrease of the nocturnal UHI in the future climate and is not able to simulate correctly the interactions and feedback between the UHI and climate change.

3.3.2. Daytime UHI

The decrease of the daytime UHI occurs with the reference, offline and inline runs, with slightly greater values for the offline run at the city centre −0.24 *versus* −0.21 °C and −0.20 °C for the reference and inline runs respectively. McCarthy *et al*. (2012) reported a decrease of the daytime UHI of London by 0.1 °C. As it can be seen from Figure 12 (bottom), there is also a decrease of the frequency of strong daytime UHI for the reference, offline and inline runs. This is mainly due to the soil drying in future climate. At mid-day, the latent heat flux
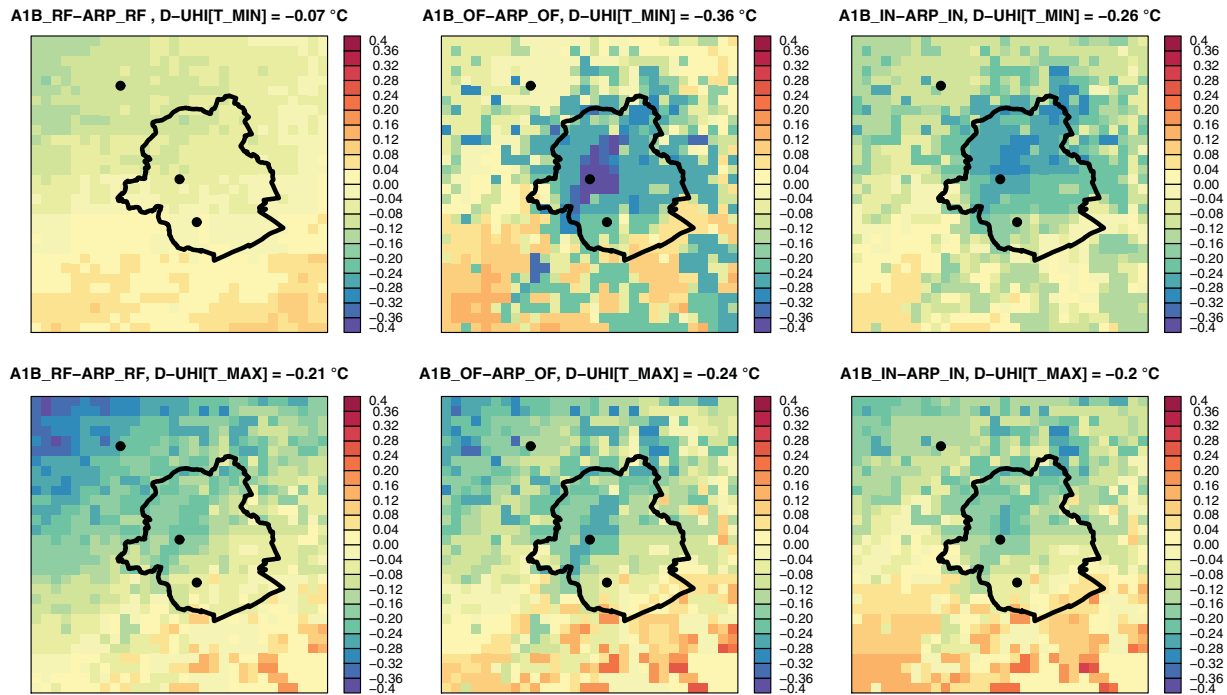
Figure 11. 2071–2100 minus 1961–1990 spatial distribution of 30-year average nocturnal (top) and daytime (bottom) UHI (°C). The three columns correspond to the reference, offline, and inline runs. The black circles indicates the location of centre of Brussels, the Uccle station situated some 6 km south of the centre of the capital in a suburban area, and the rural Brussegem station situated 20 km far away from the centre of Brussels. The UHI difference in the centre of the domain is indicated at the top of each sub-figure.

at the city centre simulated by the inline run (Figure 14) decreased by about 10 W m^{-2} by the end of century compared to present day, while rural latent heat flux decreases by about 30 W m^{-2} with the energy partitioned to sensible heat flux instead. Therefore, rural areas warm more than urban resulting in a relatively decrease in the daytime UHI. This is in agreement with the recent studies by Oleson (2012) and Lemonsu *et al.* (2013). Contrarily to what is found for the nocturnal UHI, the reference, offline, and inline runs all give similar patterns for the change of the daytime UHI in the future climate. This analysis confirms the results of McCarthy *et al.* (2010); McCarthy *et al.* (2012); Oleson *et al.* (2011); Oleson (2012); Lemonsu *et al.* (2013) that the magnitude of the UHI is not static under climate change.

3.4. Future extreme events

Heat waves have discernible impacts including rise in mortality, the frequency and occurrence of heat waves are thus vital for assessing vulnerabilities and risks to urban populations. Here, we use the definition of heat waves proposed by Huth *et al.* (2000) and employed in recent European studies (Hutter *et al.*, 2007; Kyselý *et al.*, 2010). Two thresholds, T_1 and T_2 are applied: a heat wave is defined as a continuous period of at least 5 days during which (1) T_MAX is higher than T_1 in at least 3 days, (2) mean T_MAX over the whole period is higher than T_1 and (3) T_MAX does not drop below T_2. The threshold values were set to $T_1 = 30\,°C$ and $T_2 = 25\,°C$, in accordance with the Belgian climatological practice which refers to the days with T_MAX reaching

or exceeding 30 and 25 °C as tropical and summer days, respectively. The importance of considering T_MIN was highlighted by Karl and Knight (1997) who concluded that three or more consecutive nights with no relief from very warm night time temperatures may be most important for human health impacts. In this study a third threshold T_3 was defined, with the corresponding conditions that T_MIN must be higher than T_3 in at least three nights. The threshold value was set to $T_3 = 20\,°C$ which refers to as tropical night.

Figure 15 presents the change in the number of heat wave events in the future climate calculated from the reference, offline and inline runs of the ARPEGE-Climat driven simulations for the city centre of Brussels, the Uccle suburban station, and the Brussegem rural station. As expected with the increase of the summertime temperature, heat wave events are more frequent in the future climate. The analysis of Figure 15 indicates that climate change increases the number of heat wave event in urban areas substantially more than in rural areas, confirming results of McCarthy *et al.* (2010); Oleson (2012) and Lemonsu *et al.* (2013). This is clearly a direct consequence of urban areas being warmer at night than rural areas. For the city centre, the reference and inline runs increases the number of heat wave event by a similar amount, 60 and 62 additional heat wave events, respectively. However, the offline run differs significantly with somewhat lower values (50 additional heat wave events). For the Uccle suburban area, the inline run has 58 additional heat wave events under the $2 \times CO_2$ experiment and the reference run has 53 additional heat wave events.
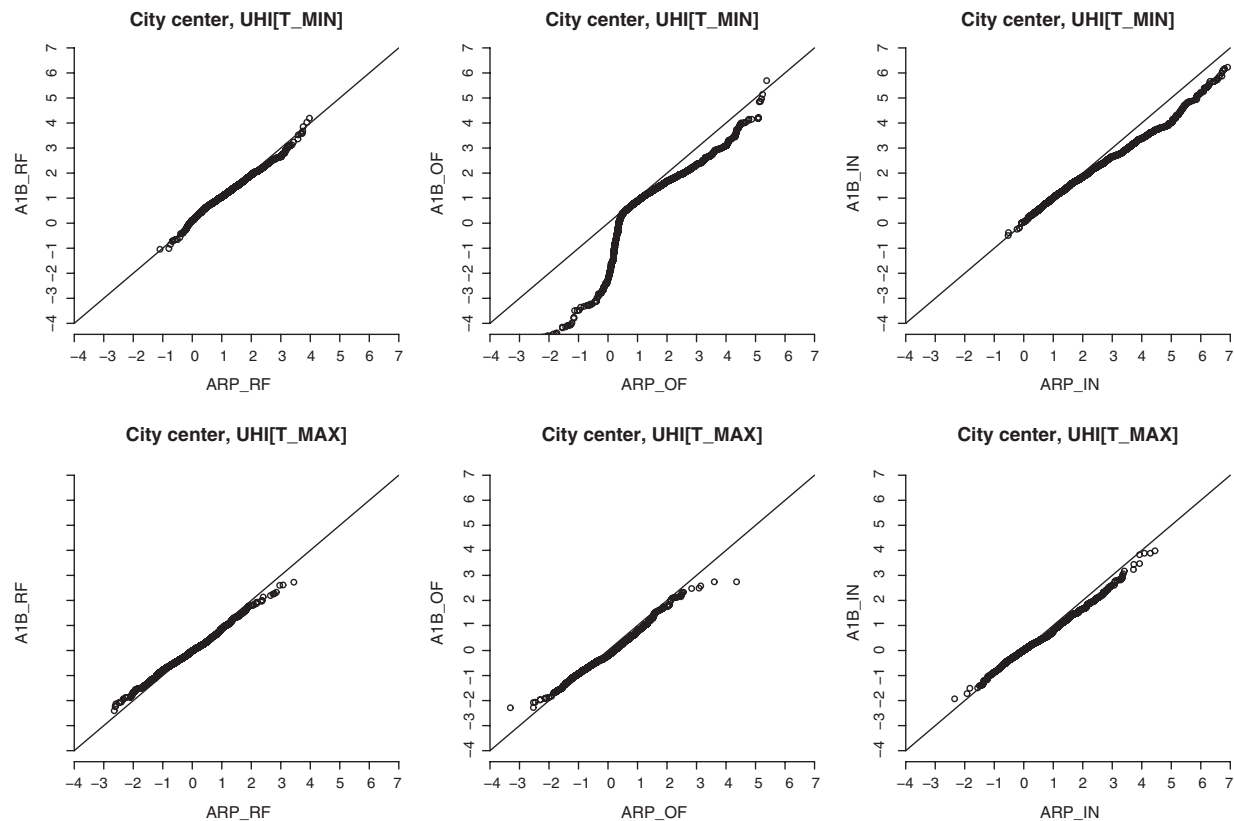
Figure 12. Quantile–quantile comparison between the nocturnal (top) and daytime (bottom) UHI (°C) at the city centre of Brussels from ARP_ and A1B_ ARPEGE-Climat driven experiment. The three columns correspond to the reference, offline and inline runs.

However, the number of heat wave event increases by similar amount for both the city centre and suburban areas with the offline run.

4. Summary and conclusions

In this study, we have proposed a new dynamical down-scaling method at 1-km horizontal resolution in order to examine how rural and urban areas might respond differently to change in future climate. The simulations have been performed with a new version of the limited-area model of the ARPEGE-IFS forecast system ALARO (Gerard *et al.*, 2009), coupled with the TEB single-layer urban canopy model (Masson, 2000) being evaluated for use as a new operational RCM for regional climate change projections over Belgium. The regional simulations have been performed first with a horizontal resolution of 40 km on a domain encompassing most of Western Europe. To increase the spatial resolution above Belgium, a nested domain has been added with 4 km resolution using the sophisticated model physics allowing the use of the ALARO model in the resolution range of 3–8 km (the so-called grey zone, Gerard *et al.*, 2009). To downscale further the regional climate projections to a urban scale, enabling a urban simulation of a city and its surrounding, the newly developed surface scheme of Météo-France SURFEX is employed in offline mode. In SURFEX, each grid box is made of four adjacent surfaces: nature, urban

areas, sea or ocean, and lake, associated with specific parameterization (e.g. TEB for urban areas, ISBA for vegetated areas). Horizontal interaction does not exist between the different surface area tiles. In this study, SURFEX is also coupled to a SBL scheme following the methodology described in Hamdi and Masson (2008) and Masson and Seity (2009). With this version, several prognostic layers are added from the ground up to the forcing level (which is the lowest ALARO level at 17 m). The SBL is, thus, resolved prognostically, taking into account large-scale forcing, turbulence, and if any, drag and canopy forces. The applicability of the method is demonstrated for the BCR, centrally located in Belgium and its UHI is defined as the difference between the urban canopy air temperature and the minimum air temperature in the surrounding rural areas. This difference is analysed for daily minimum (T_MIN) and maximum temperature (T_MAX) referred to as the nocturnal and daytime UHI. To examine the contribution and feedback processes between the UHI of the city of Brussels and the regional climate for present and future conditions, we performed downscaling simulations according to three model set-ups: (1) the reference '_RF' run representing a control simulation where the TEB scheme is not activated neither in the 4 km regional climate simulation nor in the 1 km urban climate simulation, (2) the offline '_OF' run where the TEB scheme is activated only for the 1 km urban climate simulation mimicking the situation where

Net Radiation

Sensible Heat Flux
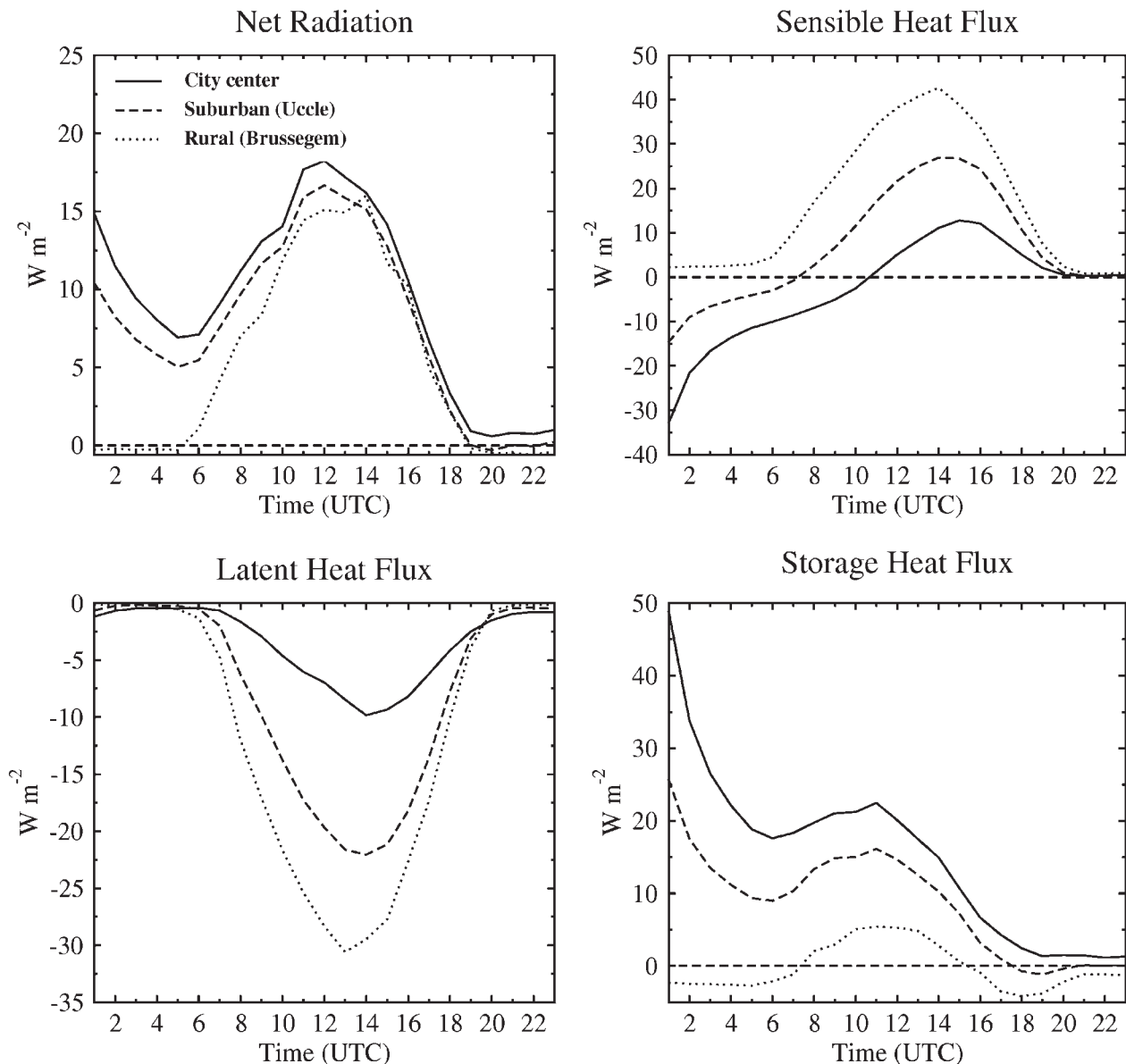

Latent Heat Flux

Storage Heat Flux

Figure 13. Summer-mean diurnal average of 2071–2100 minus 1961–1990 net radiation, sensible heat flux, latent heat flux and storage heat flux [W m^{-2}] from the offline runs of the ARPEGE-Climat driven simulations at the city centre of Brussels, the Uccle suburban station and the Brussegem rural station.

the atmospheric forcing coming from the regional climate simulations did not include any signature of the UHI and (3) the inline '_IN' run where the TEB scheme is activated both for the regional and urban climate simulations. For the simulations without TEB, urban areas are considered simply as rock and the ISBA scheme is used for all grid points of the domain. We utilized global climate scenarios from the ARPEGE-Climat (Gibelin and Déqué, 2003) GCM of Météo-France (ARP_ simulations) and we used the ARPEGE-Climat time slice 2071–2100 resulting from the IPCC SRES A1B scenario to estimate future change (A1B_ simulations). The evaluation period 1961–1990 is chosen for the comparison of observations and simulation results. Another set of simulations (ERA_ simulations) for the present climate conditions were performed using the ECMWF global reanalysis

ERA40 (Uppala *et al.*, 2005). Results from our simulations indicate the following:

Regional Climate Simulations bias

- The introduction of TEB in the regional climate simulations increases the warm bias above the BCR for both ERA40 and ARPEGE-Climat driven experiments by 0.4 °C for T_MIN and T_MAX.
- The error magnitude of T_MAX tends to be larger that T_MIN for the ARPEGE-Climat driven experiments, indicating that the correct simulation of T_MAX is more challenging during the summer.

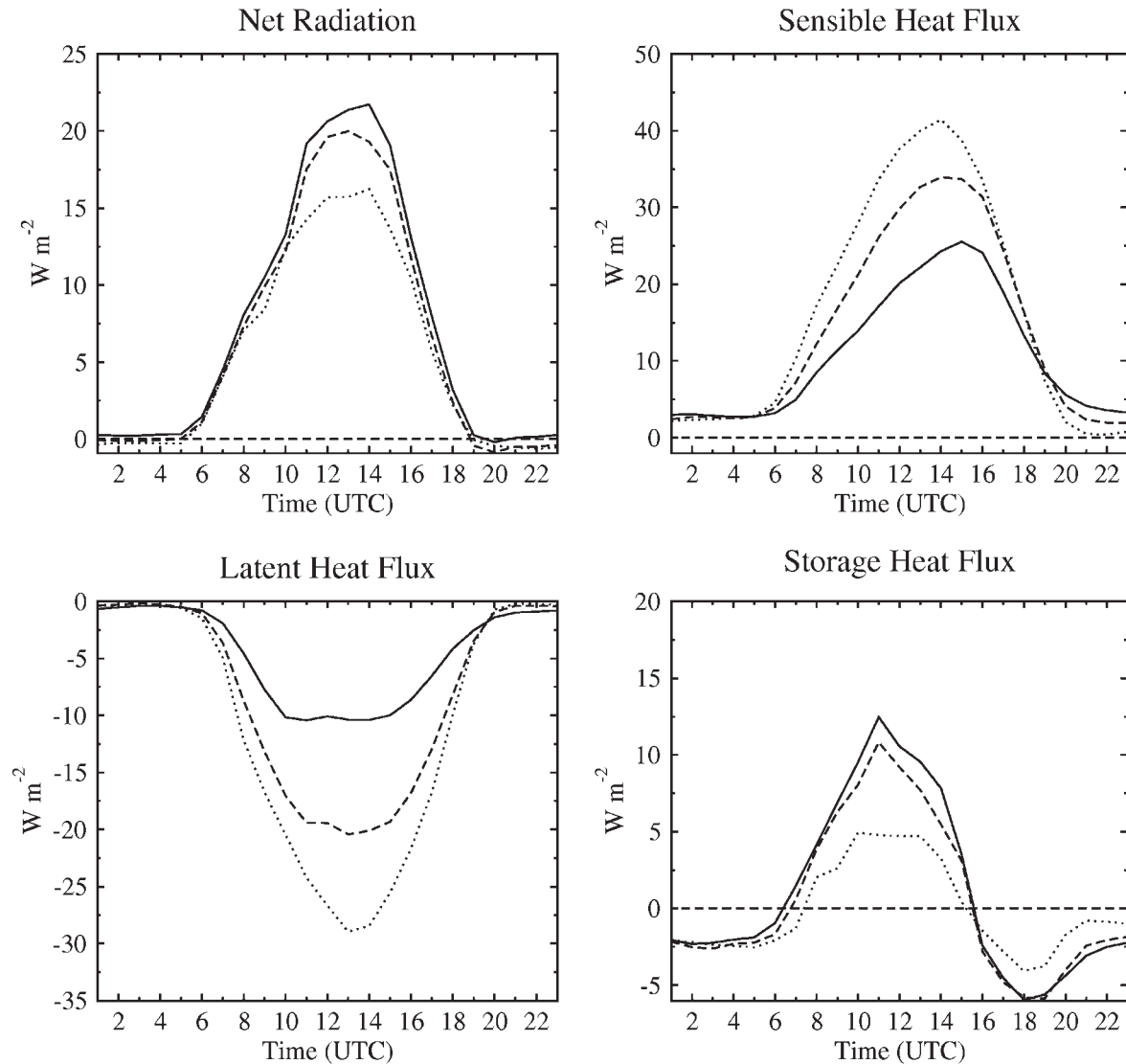Present Brussels'UHI simulated by the reference, offline and inline runs

Figure 14. Summer-mean diurnal average of 2071–2100 minus 1961–1990 net radiation, sensible heat flux, latent heat flux and storage heat flux [W m^{-2}] from the inline runs of the ARPEGE-Climat driven simulations at the city centre of Brussels, the Uccle suburban station, and the Brussegem rural station.

- Both the reference and offline runs have a comparable value of the daytime and nocturnal UHI but underestimate the UHI values calculated by the inline run.
- The ERA40 and ARPEGE-Climat driven experiments have comparable magnitude of the BCR's daytime and nocturnal UHI and a similar pattern even if the ARPEGE-Climat driven experiment has a warmer bias than the ERA40 driven simulations.
- The daytime UHI computed with the inline run is lowest in the south-eastern part of the BCR. This can be explained by the presence of the Sonian Forest. However, this feature is not reproduced neither with the reference nor with the offline run.

Validation with the observed UHI at the suburban station Uccle

- The observed UHI on minimum temperature is shown to be rising at a higher rate (2.85) than on maximum temperature with a linear trend of 0.19 °C (± 0.02 °C) and 0.06 (± 0.02 °C) (10 year)$^{-1}$ due to the increased urbanization around the Uccle station.
- This feature is not reproduced neither by the ARPEGE-Climat nor by the ERA40 driven experiments due to the lack of changes in urban extent in the model simulations.
- For the period 1981–1990, the ARP_IN nocturnal UHI agree very well with the observations, with an average value of 1.31 *versus* 1.32 °C observed, while the two other runs (ARP_RF and ARP_OF) result in much lower values with 0.78 and 0.93 °C, respectively.
- The daytime UHI computed with the ARP_RF and ARP_OF runs are comparable and negative while the ARP_IN values are positive and close to the observations.
- The reference run underestimates the warm extremes of both the nocturnal and daytime UHI by about 2 °C.
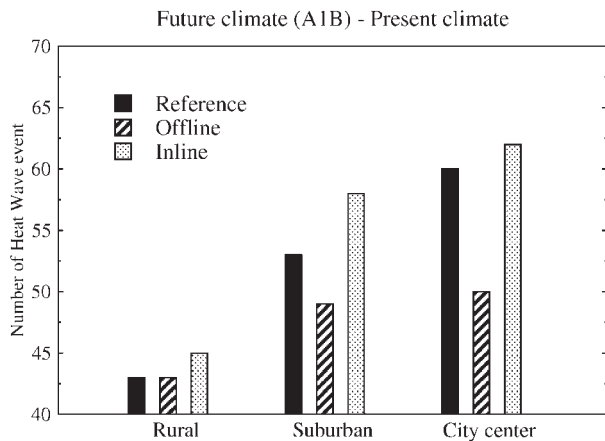
Future climate (A1B) - Present climate

Figure 15. Change in the number of heat wave event in the future climate from the reference, offline, and inline runs of the ARPEGE-Climat driven simulations at the city centre of Brussels, the Uccle suburban station, and the Brussegem rural station.

The underestimation of the nocturnal UHI is greatly reduced to less than 0.5 °C with the offline runs.

- For the daytime UHI, the offline runs reproduce the same extreme value statistics of the reference runs for both the ARPEGE-Climat and ERA40 driven experiments. The inline values are much closer to the observations.

Future Brussels's UHI characteristics

- The nocturnal UHI simulated by the reference run remains unaltered and there are no changes in either the frequency or magnitude of the extreme heat islands.
- The offline run presents a significant decrease in the nocturnal UHI over the city centre (−0.36 °C) and the suburban areas (−0.28 °C) while there is an increase over the rural areas. The frequency of present climate weak nocturnal UHI (between 0 and 1 °C) decreases to the benefit of negative UHIs in the future climate. The mechanism by which this occurs is related to changes in incoming long-wave radiation at night.
- For the inline run the nocturnal UHIs stays always positive with values between 0 and 7 °C. However, the frequency of the strong UHI (>3 °C) decreases significantly in the future climate by 1 °C. This is linked with a soil dryness during the summer where the projected cumulated summer precipitation over the BCR decreased by 35 %.
- These results indicate that the offline run exacerbates the decrease of the nocturnal UHI in the future climate and is not able to simulate correctly the interactions and feedback between the UHI and climate change.
- There is also a decrease of the daytime UHI with the reference, offline and inline runs, with slightly greater values for the offline run at the city centre −0.24 °C *versus* −0.21 °C and −0.20 °C for the reference and inline runs, respectively. There is also a decrease of the frequency of strong daytime UHI for the three runs mainly due to the soil drying in future climate.

Future extreme events

- Climate change increases the number of heat wave event in urban areas substantially more than in rural areas.
- For the city centre (suburban areas) the reference and inline runs increases the number of heat wave event by 60 (53) and 62 (58) additional heat wave events, respectively, while the offline run differs significantly with somewhat lower values (50 additional heat wave events) and similar amount for both the city centre and suburban areas.

The findings in this study show that a correct feedback of the urban heat storage to the upper atmosphere is crucial to properly simulate the UHI in past and future climate runs, therefore, we recommend the inline use of the TEB scheme. Also, these conclusions are of value to planners concerned with the uncertainty of the effects of global climate change on the climate of the BCR. However, one has to keep in mind that this is one RCM coupled to one urban parameterization, and therefore, we cannot estimate the results dispersion with respect to alternative climate change pathways or alternative global climate model. Also, the conclusion about the weakening of the urban-to-rural temperature differences in the future climate is found under the hypothesis that the bias for rural and urban areas will remain the same in the future and should, therefore, be taken with care. Another inherent limitation of these simulations is that the urban areas are static, while, in the future, urban areas are expected to increase in size. Therefore, there is a need to expand this study to include the replacement of vegetation with built surfaces.

References

Adachi SA, Kimura F, Kusaka H, Inoue T, Ueda H. 2012. Comparison of the impact of global climate changes and urbanization on summertime future climate in the Tokyo Metropolitan Area. *Journal of Applied Meteorology and Climatology* **51**: 1441–1454.
Belamari S, Pirani A. 2007. Validation of the optimal heat and momentum fluxes using the orca2-lim global ocean-ice model. *Marine environment and security for the European area. Integrated Project (MERSEA IP)*, Deliverable D4.1.3, 88.
Best MJ. 2006. Progress towards better weather forecasts for city dwellers: from short range to climate change. *Theoretical and Applied Climatology* **84**: 47–55.
Best MJ, Beljaars A, Polcher J, Viterbo P. 2004. A proposed structure for coupling tiled surfaces with the planetary boundary layer. *Journal of Hydrometeorology* **5**: 1271–1278.
Best MJ, Grimmond CSB, Villani MG. 2006. Evaluation of the urban tile in MOSES using surface energy balance observations. *Boundary-Layer Meteorology* **118**: 503–525.
Bougeault P. 1985. A simple parameterization of the large-scale effects of cumulus convection. *Monthly Weather Review* **113**: 2108–2121.
Bubnova R, Hello G, Bénard P, Geleyn JF. 1995. Integration of the fully elastic equations cast in the hydrostatic pressure terrain-following coordinate in the framework of ARPEGE/ALADIN NWP system. *Monthly Weather Review* **123**: 515–535.
Caldwell P, Chin HNS, Bader DC, Bala G. 2009. Evaluation of a WRF dynamical downscaling simulation over California. *Climatic Change* **95**: 499–521.
Changnon SA, Kunkel KE, Reinke BC. 1996. Impacts and responses to the 1995 heat wave: a call to action. *Bulletin of the American Meteorological Society* **77**: 1497–1506.

Charnock H. 1955. Wind stress over a water surface. *Quarterly Journal of Royal Meteorological Society* **81**: 639–640.

Christensen JH, Carter TR, Rummukainen M, Amanatidis G. 2007. Evaluating the performance and utility of regional climate models: the PRUDENCE project. *Climatic Change* **81**: 1–6.

Coles S. 2001. *An introduction to statistical modeling of extreme values*. Springer Verlag: London; 208.

Eliasson I. 1996. Urban nocturnal temperatures, street geometry and land use. *Atmospheric Environment* **30**: 379–392.

Fischer EM, Oleson KW, Lawrence DM. 2012. Contrasting urban and rural heat stress responses to climate change. *Geophysical Research Letters* **39**: L03705. DOI: 10.1029/2011GL050576.

Fouquart Y, Bonnel B. 1980. Computations of solar heating of the earths atmosphere: a new parameterization. *Beitraege zur Physik der Atmosphaere* **53**: 35–62.

Früh B, Becker P, Deutschländer T, Hessel JD, Kossmann M, Mieskes I, Namyslo J, Roos M, Sievers U, Steigerwald T, Turau H, Wienert U. 2011. Estimation of climate-change impact on the urban heat load using an urban climate model and regional climate projections. *Journal of Applied Meteorology and Climatology* **50**: 167–184.

Gerard L, Piriou JM, Brozková R, Geleyn JF, Banciu D. 2009. Cloud and Precipitation parameterization in a Meso-Gamma-Scale operational weather prediction model. *Monthly Weather Review* **137**: 3960–3977.

Gibelin AL, Déqué M. 2003. Anthropogenic climate change over the Mediterranean region simulated by a global variable resolution model. *Climate Dynamics* **20**: 327–339.

Giorgi F, Mearns LO. 1999. Introduction to special section: regional climate modeling revisited. *Journal of Geophysical Research* **104**(D6): 6335–6352.

Goldbach A, Kuttler W. 2013. Quantification of turbulent heat fluxes for adaptation strategies within urban planning. *International Journal of Climatology* **33**: 143–159. DOI: 10.1002/joc.3437.

Guo X, Danhong F, Jing W. 2006. Mesoscale convective precipitation system modified by urbanization in Beijing City. *Atmospheric Research* **82**: 112–126.

Hamdi R, Masson V. 2008. Inclusion of a drag approach in the Town Energy Balance (TEB) scheme: offline 1-D evaluation in a street canyon. *Journal of Applied Meteorology and Climatology* **47**: 2627–2644.

Hamdi R, Schayes G. 2008. Sensitivity study of the urban heat island intensity to urban characteristics. *International Journal of Climatology* **28**: 973–982.

Hamdi R, Deckmyn A, Termonia P, Demarée GR, Baguis P, Vanhuysse S, Wolff E. 2009. Effects of historical urbanization in the Brussels Capital Region on surface air temperature time series: a model study. *Journal of Applied Meteorology and Climatology* **48**: 2181–2196.

Hamdi R, Van de Vyver H. 2011. Estimating urban heat island effects on near-surface temperature records of Uccle (Brussels, Belgium): an observational and modeling study. *Advances in Science and Research* **6**: 27–34.

Hamdi R, Van de Vyver H, Termonia P. 2012a. New cloud and microphysics parameterization for use in high-resolution dynamical downscaling: Application for summer extreme temperature over Belgium. *International Journal of Climatology* **32**: 2051–2065. DOI: 10.1002/joc.2409.

Hamdi R, Degrauwe D, Termonia P. 2012b. Coupling the Town Energy Balance (TEB) scheme to an operational limited-area NWP model: evaluation for a highly urbanized area in Belgium. *Weather and Forecasting* **27**: 323–344.

Hassan A, Mahmoud A. 2011. Analysis of the microclimatic and human comfort conditions in an urban park in hot and arid regions. *Building and Environment* **46**(12): 2641–2656.

Hidalgo J, Masson V, Pigeon G. 2008. Urban-breeze circulation during the CAPITOUL experiment: numerical simulations. *Meteorology and Atmospheric Physics* **102**: 243–262.

Hua LJ, Ma ZG, Guo WD. 2008. The impact of urbanization on air temperature across China. *Theoretical and Applied Climatology* **93**: 179–194.

Huth R, Kyselý J, Pokornà L. 2000. A GCM simulation of heat waves, dry spells, and their relationships to circulation. *Climatic Change* **46**: 29–60.

Hutter HP, Moshammer H, Wallner P, Leitner B, Kundi M. 2007. Heatwaves in Vienna: effects on mortality. *Wiener Klinische Wochenschriften* **119**: 223–227.

Institut National de Statistique. 2009. Chiffres provisoires de la population résidente au 1er janvier, par année 1990–2009, SPF Economie—Direction Générale Statistique et Information Economique, 2009.

IPCC. 2007. Climate Change 2007. In *The Physical Science Basis. Contribution of Working Group I to the Fourth Assessment Report of the Intergovernmental Panel on Climate Change*, Solomon S, Qin D, Manning M, Chen Z, Marquis M, Averyt KB, Tignor M, Miller HL (eds). Cambridge University Press: Cambridge/New York; 996.

Jin M, Shepherd JM, Peters-Lidars C. 2007. Development of a parameterization for simulating the urban temperature hazard using satellite observations in climate model. *Natural Hazards* **43**: 257–271.

Kalnay E, Cai M. 2003. Impact of urbanization and land use on climate change. *Nature* **423**: 528–531.

Karl T, Knight R. 1997. The 1995 Chicago heat wave: how likely is a recurrence? *Bulletin of the American Meteorological Society* **78**: 1107–1119.

Koenker R. 2005. *Quantile regression*. Cambridge University Press: New York; 352.

Koenker R, Bassett G. 1978. Regression quantiles. *Econometrica* **46**: 33–50.

Kusaka H, Kondo H, Kikegawa Y, Kimura F. 2001. A simple single-layer urban canopy model for atmospheric models: comparison with multi-layer and slab models. *Boundary-Layer Meteorology* **101**: 329–358.

Kusaka H, Chen F, Tewari M, Dudhia J, Gill DO, Duda MG, Wang W, Miya Y. 2012a. Numerical simulation of Urban Heat Island effect by the WRF Model with 4-km grid increment: an inter-comparison study between the urban canopy model and slab model. *Journal of Meteorological Society of Japan* **90B**: 33–45.

Kusaka H, Hara M, Takane Y. 2012b. Urban climate projection by the WRF model at 3-km horizontal grid increment: dynamical downscaling and predicting heat stress in the 2070's August for Tokyo, Osaka, and Nagoya metropolises. *Journal of Meteorological Society of Japan* **90B**: 47–63.

Kyselý J, Picek J, Beranová R. 2010. Estimating extremes in climate change simulations using the peaks-over-threshold method with a non-stationary threshold. *Global and Planetary Change* **72**: 55–68.

Le Moigne P. 2009. SURFEX scientific documentation. Note de centre (CNRM/GMME), Météo-France, Toulouse, France, 211 pp.

Lemonsu A, Kounkou-Arnaud R, Desplat J, Salagnac JL, Masson V. 2013. Evolution of the Parisian urban climate under a global changing climate. *Climatic Change* **116**: 679–692. DOI: 10.1007/s10584-012-0521-6.

Lim YK, Shin DW, Cocke S, LaRow TE, Schoof JT, O'Brien JJ, Chassignet EP. 2007. Dynamically and statistically downscaled seasonal simulations of maximum surface air temperature over the southeastern United States. *Journal of Geophysical Research* **112**, D24102. DOI: 10.1029/2007JD008764.

Lorenz EN. 1969. The predictability of a flow which possesses many scales of motion. *Tellus* **3**: 289–307.

Lynn BH, Carlson T, Rosenzweig C, Goldberg R, Druyan L, Cox J, Gaffin S, Parshall L, Civerolo K. 2009. A modification to the NOAH LSM to simulate heat mitigation strategies in the New York City Metropolitan area. *Journal of Applied Meteorology and Climatology* **48**: 199–216.

Lynn BH, Rosenzweig C, Goldberg R, Rind D, Hogrefe C, Druyan L, Healy R, Dudhia J, Rosenthal J, Kinney P. 2010. Testing GISS-MM5 physics configurations for use in regional impacts studies. *Climatic Change* **99**: 567–587.

Martilli A, Clappier A, Rotach MW. 2002. An urban surface exchange parameterization for mesoscale models. *Boundary-Layer Meteorology* **104**: 261–304.

Martine G, Marshall A. 2007. *State of world population 2007: Unleashing the potential of urban growth, report*. U. N. Popul Fund: New York.

Masson V. 2000. A physically-based scheme for the urban energy budget in atmospheric models. *Boundary-Layer Meteorology* **94**: 357–397.

Masson V. 2006. Urban surface modeling and the meso-scale impact of cities. *Theoretical and Applied Climatology* **84**: 35–45.

Masson V, Seity Y. 2009. Including atmospheric layers in vegetation and urban offline surface schemes. *Journal of Applied Meteorology and Climatology* **48**: 1377–1397.

Masson V, Champeaux JL, Chauvin F, Meriguet C, Lacaze R. 2003. A global database of land surface parameters at 1km resolution in meteorological and climate models. *Journal of Climate* **16**: 1261–1282.

McCarthy MP, Best MJ, Betts RA. 2010. Climate change in cities due to global warming and urban effects. *Geophysical Research Letters* **37**: L09705. DOI: 10.1029/2010GL042845.

McCarthy MP, Harpham C, Goodess CM, Jones PD. 2012. Simulating climate change in UK cities using a regional climate model,

HadRM3. *International Journal of Climatology* **32**: 1875–1888. DOI: 10.1002/joc2402.

Miao S, Chen F, LeMone M, Tewari M, Li Q, Wang Y. 2009. An observational and modeling study of characteristics of urban heat island and boundary layer structures in Beijing. *Journal of Applied Meteorology and Climatology* **48**: 484–501.

Mlawer EJ, Taubman SJ, Brown P, Iacono MJ, Clough SA. 1997. Radiative transfer for inhomogeneous atmospheres: RRTM, a validated correlated-k model for the longwave. *Journal of Geophysical Research* **102**: 16 663–16 682.

Morcrette JJ. 1991. Radiation and cloud radiative properties in the ECMWF operational weather forecast model. *Journal of Geophysical Research* **9121–9132**.

Moss RH *et al.* 2010. The next generation of scenarios for climate change research and assessment. *Nature* **463**: 747–756.

Ng E, Chen L, Wang Y, Yuan C. 2012. A study on the cooling effects of greening in a high-density city: an experience from Hong Kong. *Building and Environment* **47**(1): 256–271.

Nicolis C. 2003. Dynamics of model error: some generic features. *Journal of the Atmospheric Sciences* **60**: 2208–2218.

Nicolis C. 2004. Dynamics of model error: role of unresolved scale revisited. *Journal of the Atmospheric Sciences* **61**: 1740–1753.

Noilhan J, Planton S. 1989. A simple parameterization of land surface processes for meteorological models. *Monthly Weather Review* **117**: 536–549.

Oke TR, Johnson GT, Steyn DG, Watson ID. 1991. Simulation of surface urban heat islands under "Ideal" conditions at night Part 2: diagnosis of causation. *Boundary-Layer Meteorology* **56**: 339–358.

Oleson K. 2012. Contrasts between urban and rural climate in CCSM4 CMIP5 climate change scenarios. *Journal of Climate* **25**: 1390–1412.

Oleson KW, Bonan GB, Feddema J, Jackson T. 2011. An examination of urban heat island characteristics in a global climate model. *International Journal of Climatology* **31**: 1848–1865.

Paquin-Ricard D, Jones C, Vaillancourt PA. 2010. Using ARM observations to Evaluate cloud and clear-sky radiation processes as simulated by the Canadian regional climate model GEM. *Monthly Weather Review* **138**: 818–838.

Pearlmutter D, Krüger EL, Berliner P. 2009. The role of evaporation in the energy balance of an open-air scaled urban surface. *International Journal of Climatology* **29**(6): 911–920.

Peters EB, Hiller RV, McFadden JP. 2011. Seasonal contributions of vegetation types to suburban evapotranspiration. *Journal of Geophysical Research G: Biogeosciences* **116**(1): G01003.

Pigeon G, Moscicki MA, Voogt JA, Masson V. 2008. Simulation of fall and winter surface energy balance over a dense urban area using the TEB scheme. *Meteorology and Atmospheric Physics* **102**: 159–171.

Qian JH, Seth A, Zebiak S. 2003. Reinitialized versus continuous simulations for regional climate downscaling. *Monthly Weather Review* **131**: 2857–2874.

Rosenzweig C, Solecki W, Hammer SA, Mehrotra S. 2010. Cities lead the way in climate-change action. *Nature* **467**: 909–911.

Sardon JP. 2007. The 2003 heat wave. *Euro Surveillance* **12**(3): 694.

Simmons A, Burridge DM. 1981. An energy and angular-momentum conserving finite-difference scheme and hybrid vertical coordinates. *Monthly Weather Review* **109**: 758–766.

Sutton PC, Anderson SJ, Elvidge CD. 2009. Paving the planet: impervious surface as proxy measure of the human ecological footprint. *Progress in Physical Geography* **33**: 510–527.

Termonia P, Voitus F, Degrauwe D, Caluwaerts S, Hamdi R. 2012. Application of Boyd's periodization and relaxation method in a spectral atmospheric limited-area model - Part I : implementation and reproducibility tests. *Monthly Weather Review* **140**: 3137–3148. DOI: :10.1175/MWR-D-12-00033.1.

Trusilova K, Jung M, Churkina G, Karstens U, Heimann M, Claussen M. 2008. Urbanization impact on the climate in Europe: Numerical experiments by the PSU-NCAR mesoscale model (MM5). *Journal of Applied Meteorology and Climatology* **47**: 1442–1455.

Uppala SM, Kallberg PW, Simmons AJ, Andrae U, da Costa BV, Fiorino M, Gibson JK, Haseler J, Hernandez A, Kelly GA, Li X, Onogi K, Saarinen S, Sokka N, Allan RP, Andersson E, Arpe K, Balmaseda MA, Beljaars ACM, van de Berg L, Bidlot J, Bormann N, Caires S, Chevallier F, Dethof A, Dragosavac M, Fisher M, Fuentes M, Hagemann S, Holm S, Hoskins BJ, Isaksen L, Janssen PAEM, Jenne E, McNally AP, Mahfouf JF, Morcrette JJ, Rayner NA, Saunders RW, Simon P, Sterl A, Trenberth KE, Untch A, Vasiljevic D, Viterbo P, Woollen J. 2005. The ERA-40 re-analysis. *Quarterly Journal of Royal Meteorological Society* **131**: 2961–3012.

Van de Vyver H. 2012. Evolution of extreme temperature in Belgium since the 1950s. *Theoretical and Applied Climatology* **107**: 113–129. DOI: 10.1007/s00704-011-0456-2

Van Weverberg K, De Ridder K, Van Rompaey A. 2008. Modeling the contribution of the Brussels Heat Island to a long temperature time series. *Journal of Applied Meteorology and Climatology* **47**: 976–990.

Yan Z, Jones PD, Davies TD, Moberg A, Bergström H, Camuffo D, Cocheo C, Maugeri M, Demarée GR, Verhoeve T, Thoen E, Barriendos M, Rodríguez R, Martín-Vide J, Yang C. 2002. Trends of extreme temperatures in Europe and China based on daily observations. *Climatic Change* **53**: 355–392.

Zhang CL, Chen F, Miao SG, Li QC, Xia XA, Xuan CY. 2009. Impacts of urban expansion and future green planting on summer precipitation in the Beijing metropolitan area. *Journal of Geophysical Research* **114**: D02116.